

**ELASTOMERLERİN SAYISAL YÖNTEMLERLE ANALİZİ VE
ŞEKİLSEL DÖKÜM YÖNTEMİ İLE DARBELERE DAYANIKLI
ROBOT GELİŞTİRİLMESİ**

**NUMERICAL ANALYSIS AND MANUFACTURING OF
ELASTOMERS UTILIZING SHAPE DEPOSITION
MANUFACTURING METHOD TO DESIGN A RUGGED
ROBOT**

BEHRANG SHAMSADINLO

DR. ÖZGÜR ÜNVER
Supervisor

Submitted to the Institute of Science of Hacettepe University
As a Partial Fulfillment to the Requirements
For the Award of the Degree of Master of Science
In Mechanics

2013

This work named “ **Numerical Analysis and Manufacturing of Elastomers Utilizing Shape Deposition Manufacturing Method to Design a Rugged Robot**” by **BEHRANG SHAMSADINLO** has been approved as a thesis for the degree of **Master of Science** in Mechanic by below mentioned Examining Committee Members.

Asst. Prof. Benat KOÇKAR
Head

Dr. Özgür ÜNVER
Supervisor

Asst. Prof. Tuncay KARAÇAY
Member

This thesis has been approved as a thesis for the Degree of **MASTER OF SCIENCE IN MECHANICS** by Board of Directors of the Institute for Graduate Studies in Science and Engineering.

Prof. Dr. Fatma SEVİN DÜZ
Director of the Institute of Graduate Studies in Science

To my family

ETHICS

In this thesis study, prepared in accordance with the spelling rules of Institute of Graduate Studies in Science of Hacettepe University,

I declare that

- all the information and documents have been obtained in the base of the academic rules
- all audio-visual and written information and results have been presented according to the rules of scientific ethics
- in case of using others Works, related studies have been cited in accordance with the scientific standards
- all cited studies have been fully referenced
- I did not do any distortion in the data set
- and any part of this thesis has not been presented as another thesis study at this or any other university.

16/12/2013

BEHRANG SHAMSADINLO

ÖZET

ELASTOMERLERİN SAYISAL YÖNTEMLERLE ANALİZİ VE ŞEKİLSSEL DÖKÜM YÖNTEMİ İLE DARBELERE DAYANIKLI ROBOT GELİŞTİRİLMESİ

Behrang SHAMSADINLO

Yüksek Lisans, Makina Mühendisliği Bölümü

Tez danışmanı: Dr. Özgür Ünver

Aralık, 2013

Günümüzde kullanımları eksponansiyel olarak artan mekatronik uygulamalar ve robotlar her geçen gün daha hızlı, akıllı ve kullanışlı olmaktadır. Yeni nesil robotlar gövdelerinde bir çok kamera, algılayıcı ve eyleyici gibi yüksek ivme ve gerilim altında kırılabilir parçalarla çalışmaktadır. Bu tezin amacı; halihazırda tedarik edilen algılayıcı ve eyleyicilerin elastomerik malzemelerin içine gömülmesi ile robotların çok daha dayanıklı hale getirilmesidir. Bu proje kapsamında hızlı prototipleme yöntemlerinden biri olan Şekilsel Döküm ve Üretim Yöntemi (ŞDÜ) kullanılmıştır.

Bu tez kapsamında; yüksek aşınma direnci, yırtılma direnci, kimyasal direnç, mikrobiyal direnç ve ayarlanabilir Shore sertliği nedenleri ile hızlı hareketlerde viskoelastik özelliği, yüksek deformasyonda ise hiperelastik özellik gösteren poliüretanın kullanılmasına karar verilmiştir.

Bu tezin hedefi; malzemelerin viskoelastik ve hiperelastik özelliklerini kullanarak darbelere karşı dayanıklı bir robot geliştirme algoritmasının bulunmasıdır. Bu amaç doğrultusunda; seçilen elastomerik malzemeler Sonlu Elemanlar Yöntemi ve Yapay Sinir Ağı gibi sayısal yöntemler kullanılarak analiz edilmiştir. Sonlu elemanlar modelini oluşturmak için tek eksenli çekme, kesme, iki eksenli çekme gibi test sonuç bilgilerine ihtiyaç vardır. Ancak kesme ve iki eksenli çekme testleri çok nadir bulunan ve pahalı test cihazları tarafından gerçekleştirilebilmektedir. Bu yüzden, bu testler fiziksel olarak

gerçekleştirilmemiş, yerine Valanis-Landel yöntemi ile çekme ve basma test verileri kullanarak yaklaşık sonuçlar bulunmuştur.

Elde edilen tüm sonuçların test edilmesi ve modellerle karşılaştırılması amacıyla bu tez kapsamında düşme test cihazı tasarlanmış ve üretilmiştir. Bu test düzeneği ile farklı alan ve kalınlıklara sahip malzemeler farklı değişik hız ve ağırlıklarla test edilmiş, böylece tüm bu değişkenlerin malzeme üzerinde oluşturduğu azami ivme ve gerilme değerleri üzerine olan etkileri belirlenmiştir.

Anahtar kelimeler: Poliüretan Elastomer, Sonlu Elemanlar Yöntemi, Hiperelastik ve Viskoelastik Malzemeler, Şekilsel Döküm ve Üretim.

ABSTRACT

NUMERICAL ANALYSIS AND MANUFACTURING OF ELASTOMERS UTILIZING SHAPE DEPOSITION MANUFACTURING METHOD TO DESIGN A RUGGED ROBOT

Behrang SHAMSADINLO

Master of Science, Department of Mechanical Engineering

Supervisor: Dr. Özgür ÜNVER

December, 2013

The robotic and its evolution in recent years is one of the most transformative inventions of man. Over years innovations have made robots faster, more intelligent and smart. Modern robots utilize increasing numbers of cameras, sensors, actuators and etc. Some of these mechatronic devices are sensitive to applied acceleration and/or stress. More electronic devices are expected to provide more functionality whilst remaining safe when using in harsh environment. In this thesis, the ultimate goal is to design a rugged robot which provides maximum level of protection for sensitive components. This performance would be satisfied by embedding the electronic devices into a host objects made by rubber-like materials; which are widely used in decreasing intensity of impact loads or acceleration. Polyurethane elastomers are viscoelastic rubber-like materials with very wide shore hardness which provide different dynamic properties. These materials are selected due to their superior properties such as; viscoelastic behavior under high strain rates and elastic behavior under low strain-rates.

Embedding of the components in the host material requires special manufacturing method to manufacture the robot in 3-D and monolithic way. We used a special rapid prototyping method named Shape Deposition Manufacturing (SDM) to manufacture the robot.

The main objective of this thesis is to design a rugged robot by analyzing viscoelastic and hyperelastic behaviors of the material. Numerical methods such as Finite Element Method (FEM) and Neural network are implemented to analyze the behavior of material under different loading conditions. FEM requires data-set results of materials from multiple test set-ups (uniaxial tension, pure shear, biaxial). Shear and biaxial tests require special mechanical devices that are scarce and expensive, therefore; an alternative Valanis-Landen method was used instead of performing these tests.

To analyze the realistic impact, a test device is designed to test the specimens with different area and thickness under different testing conditions of drop height and drop mass. Finally, the best design parameters are selected to ensure protection of the rugged robot.

Keywords: Polyurethane Elastomer, Finite Element Method, Hyperelastic and Viscoelastic Analysis, Shape Deposition Manufacturing.

TEŐEKKÜR

Yüksek lisans eğitimime ilk başladığım andan itibaren özveriyle bilgisini, sabrını ve insani ilgisini esirgemeyen tez danışmanım Dr. Özgür Ünver'e, yeni çıkacağım bu yolda sonsuz desteđi için teşekkürler.

Ayrıca, başta Sayın Yrd. Doç. Dr. Benat Koçkar ve Prof. Bora Yıldırım ve olmak üzere, yüksek lisans eğitimim süresince üzerimde emeđi geçen Hacettepe Üniversitesi Makine Mühendisliđi Bölümü'ndeki bütün akademisyenlere teşekkür ederim. Aynı zamanda, tez komitesinde jüri üyeliđinde bulunan Sayın Yrd. Doç. Dr. Tuncay Karaçay'a tezime gösterdiđi ilgi için çok teşekkür ederim.

Yüksek lisansım süresince çalıştığım Hacettepe Makine Mühendisliđi bölümündeki Senstech Laboratuvarındaki çalışma arkadaşlarıma göstermiş oldukları yardımları ve dostlukları için çok teşekkür ederim. Yüksek lisansta her zaman yanımda olan Peyman Ansari ve Morteza Dusti'ye teşekkürler. Ayrıca yüksek lisans süresinde beraber bir evde yaşadığımız Rashad Qafarov ve kardeř gibi her zaman yanımda olan Mehdi Mazaheri'den çok teşekkür ederim.

Hayatımda her zaman yanımda olan ve benden maddi ve manevi hiçbir desteđi esirgemeyen babama ve anneme çok teşekkür ederim. Yüksek lisansım süresince manevi desteklerinden dolayı abim Ali'ye de teşekkür ederim.

CONTENTS

	<u>Page</u>
ÖZET	i
ABSTRACT	iii
TEŞEKKÜR	v
CONTENTS.....	vi
LIST OF TABLES	viii
LIST OF FIGURES.....	viii
NOMENCLATURE	x
1. INTRODUCTION	1
1.1. Problem Statement.....	1
1.2. Research Goal and Objectives.....	1
1.3. Challenges	2
1.4. Outline	3
2. LITERATURE SURVEY	4
2. 1. Definition of the Critical Issues	4
2. 2. Analyzing the Hyperelasticity and Viscoelasticity of Materials.....	5
2.2.1. Hyperelastic Material Models	10
2.2.1.1. Mooney-Rivlin.....	11
2.2.1.2. Ogden.....	12
2.2.1.3. Neo-Hookean	12
2.2.1.4. Gent.....	13
2.2.2. Experimental set-up	14
2.2.2.1. Details of the Material.....	15
2.2.2.2. Uniaxial Tension Test.....	16
2.2.2.3. Biaxial Test.....	18
2.2.2.4. Shear Test.....	20
2.2.2.5. Drop Test Device.....	21
2.3. Manufacturing Process.....	25
2.3.1. Shape Deposition Manufacturing (SDM)	25

2.3.2. CAD Model Creation.....	26
2.3.3. Materials in SDM	27
2.3.3.1. Part material	28
2.3.3.2. Support Material	29
2.3.3.3. Temporary Material	29
2.3.3.4. Sacrificial Material	29
2.3.3.5. Embedded Components.....	29
2.3.3.6. General Considerations in Material Selection.....	31
2.3.3.7. Effective Parameters on Changing Mechanical Properties of Elastomers....	33
2.3.3.7.1. Cure time.....	33
2.3.3.7.2. Mixing time	34
2.3.3.7.3. Annealing	34
2.3.3.7.4. Creep.....	36
2.3.3.7.5. Stress softening (Mullins effect)	36
2.3.4. Different Manufacturing Process of SDM	37
3.3.5. Fixturing Challenges for Flexible Components	38
3. RESULTS AND DISCUSSIONS.....	40
3.1. Operations on Material	40
3.2. Increasing SDM Performance	41
3.3. Finding constants of Hyperelastic Materials	43
3.3.1. Constants of Mooney-Rivlin.....	43
3.3.2. Constants of Ogden	44
3.3.3. Constants of Neo-Hookean	44
3.3.4. Constants of Gent	44
3.4. Results of FEA	45
3.4.1. Data-set Combination Effect on Different Material Models in Uniaxial Tension Test	46
3.4.2. Data-set Combination Effect on Different Material Models in Shear Test.....	48
3.5. Comparing Different Material Model Results	50
3.6. Impact Modeling	53
3.6.1. Modeling of PD.....	54

3.6.1.1. Analytical Model of PD	54
3.6.1.2. Empirical Modeling (NN method).....	57
3.6.1.3. Comparison of Analytical and Empirical Modeling.....	60
3.6.2. Stress Analysis	61
3.6.2.1. Differential Equation	61
3.6.2.2. Finite Element Method.....	62
3.6.2.3. Comparison of FEM and Differential Equation	65
4. CONCLUSIONS	66
4.1. Improving SDM.....	66
4.2. Analyzing a Hyperelastic Material using FEM	66
4.3. Impact Analyzes of Viscoelastic Material.....	67
4.4. Future Works.....	67
REFERENCES.....	68
APPENDIX	71
CURRICULUM VITAE	75

LIST OF TABLES

Table 2.1. Mechanical properties of the V10 polyurethane elastomer	15
Table 2.2. Specimens manufactured for testing	23
Table 2.3. Sample variables and PD results of specimens	24
Table 2.4. Examples of mechanical properties of elastomeric polyurethanes.	28
Table 3.1. Tension test on specimens with different contact area	42
Table 3.2. 2 and 9-parameter Mooney-Rivlin constants	44
Table 3.3. RMS error of material models for each test models.....	52
Table 3.4. The artificial NN structure	58
Table 3.5. Specimens manufactured for testing	60
Table 3.6. RMS error of each model	60

LIST OF FIGURES

Figure 2.1. Schematic diagram of the behavior of the elastomer in simple shear [7] ..	6
Figure 2.2. Middle cross section of entire structure [10]	7

Figure 2.3. The multi-layered buffering system with embedded SIP [4]	8
Figure 2.4. Nonlinear impact model [12].....	9
Figure 2.5. A photo of the uniaxial tension test machine during testing in approximately 300% of elongation (left) and the drawing of the specimen (right)	17
Figure 2.6. Estimated results of biaxial tension test using the equivalent equation and VL function	19
Figure 2.7. A photo of the uniaxial compression test (left) and the drawing of the specimen (right).....	20
Figure 2.8. Comparison of pure shear test and corresponding VL function results. ..	21
Figure 2.9. A photo of the designed drop test; cylindrical bearing (1), impact rig (2), adjustable mass (3), Specimen (4), and accelerometer (5).....	22
Figure 2.10. A sample plot of the impact deceleration of a specimen, where; $A=28.26$ cm ² , $T=5.19$ mm, $M=1.866$ kg and $H= 5$ cm versus time	23
Figure 2.11. The manufacturing process of the SDM	25
Figure 2.12. The SDM cyclic process involving material addition and removal and component embedding.....	26
Figure 2.13. An example of SDM manufacturing process: Designing (A), Embedding process after machining the mold (B), Deposit part material (C), Machining (D), and Releasing from mold (E). [30].....	27
Figure 2.14. Sacrificial material (yellow), support material (blue) and embedded components [30].....	30
Figure 2.15. Example of embedded components Double-Jointed compliant leg (fabricated by SDM) [30].....	31
Figure 2.16. Polyurethane used as a part material.....	33
Figure 2.17. Effect of annealing on arrangement of domains [40].....	35
Figure 2.18. Annealing device	35
Figure 2.19. Creep effect [40].....	36
Figure 2.20. Mullins effect [18]	37
Figure 3.1. Plot of elongation vs. time (days)	40
Figure 3.2. Plot of load/thickness vs. time (days)	41
Figure 3.3. Bonding of two different materials	42
Figure 3.4. The block diagram of ANSYS analysis.....	46
Figure 3.5. FEA of the uniaxial tension test using Mooney-Rivlin (9-parameter) model	47
Figure 3.6. FEA of the uniaxial tension test using Ogden 1rd model.....	47
Figure 3.7. FEA of the uniaxial tension test using Neo-Hookean model.....	48
Figure 3.8. FEA of the uniaxial tension test using Gent model.....	48
Figure 3.9. FEA of the pure shear test using Mooney-Rivlin (9-parameter) model....	49
Figure 3.10. FEA of the pure shear test using Ogden (1-rd) model.....	49
Figure 3.11. FEA of the pure shear test using Gent model	50
Figure 3.12. FEA of the pure shear test using Neo-Hookean model	50

Figure 3.13. Difference of material models in analyzing uniaxial tension test.....	51
Figure 3.14. Difference of material models in analyzing shear test	51
Figure 3.15. An example plot of PD vs. thickness with different drop height	54
Figure 3.16. A best fit plot of deceleration ratio vs. thickness.....	55
Figure 3.17. A best fit plot of deceleration ratio vs. Area	56
Figure 3.18. A best fit plot of deceleration ratio vs. mass	56
Figure 3.19. A best fit plot of PD vs. height	57
Figure 3.20. Regression analysis of MPL network.	59
Figure 3.21. Performance of the NN.....	59
Figure 3.22. 3-D analyzing the drop test in ANSYS.....	64
Figure 3.23. Von-misses stresses over time during an impact	64
Figure 3.24. A plot of comparison of calculated stresses.	65
Figure 3.25. A plot of stress vs. mass	65

NOMENCLATURE

λ	Principal stretch ratio
ε	Engineering strain
σ	Engineering stress
T	True stress
t	Thickness of specimen
L	Gage Length of specimen
A	Cross section area of specimen
D	Diameter of specimen
$C_{10}, C_{01}, \dots, C_{nn}$	Constants of Mooney-Rivlin material model
\bar{I}_1, \bar{I}_2	First and second deviatoric strain invariant
d	Material incompressibility
J	Determinant of the elastic deformation gradient

w	Strain energy density function value
μ	Initial shear modulus
α_r	Ogden material model constant
μ_r	Ogden material model constant
μ	Gent material model constant
J_m	Gent material model constant
$T(t)$	Thickness function
$A(a)$	Area function
$M(m)$	Mass function
$H(h)$	Drop height function
σ_0	Static stress

1. INTRODUCTION

1.1. Problem Statement

Nowadays many robots are manufactured for various applications. Some of these robots work in real environment conditions which increased risk of damage. Most of robots are sensitive and have potential of receiving large damages in very small impacts, falling from height, rolling over or collisions. In this thesis we are trying to find a way to overcome these problems. Sometimes increasing material or using another soft material (as a protector) around the sensitive object considered to increase robustness. However, there is an alternative method which enables us to embed different mechanic and electronic parts of the robot in a soft viscoelastic material using shape deposition manufacturing (SDM) method.

Protecting of products plays significant role in engineering and almost in every industry. It leads to generate the science of packaging. In this study protection of sensitive robot components is considered. Some of the sensors are sensitive to applied acceleration. In this thesis, the Peak deceleration (PD) of the applied impact load is modeled empirically, analytically and compared with experimental data. Also the maximum stress on the material is calculated using the Finite Element Method (FEM).

1.2. Research Goal and Objectives

The main objective of this study is to model viscoelastic material behavior under Impact loads to design a rugged robot which could endure external impact loads. This thesis presents the methods of manufacturing rugged robots. Moreover, all dynamic and physical conditions are explored and documented in this work. Following questions will be answer in this study:

- What type of materials should be used to provide maximum protection for sensitive components?

- How to enhance the mechanical properties of a material?
- Which parameters of the material are more important to reach the robustness?
- How to manufacture integrated components without using screws, washers, and nuts?
- How to protect sensitive components from impacts?
- How to manufacture objects with less than a millimeter-scale?
- How to interface two different elastomers?
- How to model viscoelastic material?
- How do thickness and area of the specimen affect the peak deceleration?
- How do the robot weight and speed affect the peak deceleration?
- How to model the dynamic behavior of the material?
- How to reach the stress on the material from the peak deceleration?
- How to model the Peak Deceleration (PD) analytically and numerically?
- How to analyze these materials in ANSYS?
- Which material model must be used for modeling the hyperelastic material using Finite Element Analysis (FEA)?
- How to predict the stress-strain of the material under shear and biaxial test without perform a test
- Which combination of a data-set could solve the model more precisely?
- Which combination of a data-set has the best results?

1.3. Challenges

There are lots of problems in numerically analyzing the material behavior of the elastomeric polyurethane in ANSYS. Numerical modeling of the specimen using finite element method requires adequate experimental data-sets in three different test set-ups. Three experimental set-ups are: uniaxial tension, uniaxial simple shear and biaxial tension tests. Unfortunately, shear and biaxial tests need special test setups that are rarely found and expensive. In order to compensate the lack of experimental data, an estimation method could be used to predict experimental data set of shear

and biaxial without practically performing these tests. For this purpose the Valanis-Landel method is used. Shear and biaxial data-sets are predicted from uniaxial tension and uniaxial compression tests which are mostly available in all laboratories.

Another problem is modeling the dynamic behavior of the elastomers. Modeling of the viscoelastic material as a spring and damper is really hard and is not very applicable. On the other hand, the specimen spring constant and damping coefficient are fully related to the specimen size and testing conditions. Since the peak deceleration is needed to model in this work; a special test device designed and manufactured. By using this test device, the Peak Deceleration (PD) and Stress is modeled according to specimen size and testing conditions. The biggest problem in PD of the specimens in drop test is the maximum measurable acceleration of the accelerometer that affects the measurable impact range of constitutive material modeling.

1.4. Outline

In this study, next section is devoted to the literature review. Then, section 3 is allocated for results of analytical and numerical solution of PD and stress of polyurethane elastomers; afterwards, characterization of different material models and different combinations are presented. Finally, section 4 is dedicated to the conclusion.

2. LITERATURE SURVEY

2. 1. Definition of the Critical Issues

Many researchers have been used the viscoelastic materials to protect embedded electronic systems under impact loads [1-4]. In [4] for instance; a numerical model of an electronic system, which is embedded in multiple viscoelastic materials under impact loads, was studied. According to the work, a design methodology is defined for buffer layers of viscoelastic material which significantly increased the protection of embedded electronic systems. The effect of the thickness of different viscoelastic buffer layers on decreasing the stress on the electronic circuits was investigated using Finite Element Method (FEM). However, authors compared two thicknesses only. It is numerically proven that the thickness of the viscoelastic materials would dramatically affect the maximum stress on the material [4].

Since we do not have chance to test all the materials with all variables at any time, we need a model to find the impact forces and peak decelerations (PD) in colliding bodies. It is difficult to determine the impact forces using elastic stress wave theory [1]. Dan K. Song [5] has worked on modeling the impact phenomena and predicting the impact force when a mass experiences a collision to a contact pad. The elastomeric contact pad is modeled as a linear and nonlinear spring and nonlinear a damper. In another work [6], the viscoelastic contact pad is modeled as linear and/or nonlinear contact stiffness. These studies [5][7] model the impact force when an ideal mass with a constant area experiences a collision at different heights only. Few studies have been investigated to examine the effects of physical parameters such as; specimen size, temperature, drop mass, density and etc. on impact modeling of the viscoelastic materials so far. J. A. Sherwood, *et al* [7] have been worked on modeling the compressive stress-strain response of polyurethane foam under compressive impact loads considering the effects of density, temperature and strain rate as separable functions.

Modeling the behavior of the viscoelastic material would enable us to reach desired protection. Further, it could help us to design the protective material size. There are many investigations on modeling the behavior of the material under low strain rates which known as hyperelastic material modeling [8-11] and high strain rates which calls viscoelasticity. In this study, different material models behavior is analyzed in details.

Finding a best material, modeling its dynamic behavior, finding the ideal specimen size to protect the embedded components of the robot and defining the special manufacturing process (SDM) are the purpose of this study. Each goal is introduced briefly in the next sections.

SDM process is a useful method for manufacturing 3-D models with extremely complex geometries in very high accuracy [12]. The SDM is appropriate manufacturing process for pourable materials such as polyurethane elastomer which is used in this study.

2. 2. Analyzing the Hyperelasticity and Viscoelasticity of Materials

The polyurethane elastomers are widely used materials in many areas such as; aerospace, automotive, civil engineering and medical field due to their superior properties such as; viscoelastic behavior under high strain rates, elastic behavior under large deformations and abrasion, cut, microbial, chemical resistance and etc. When the load is applied to a material, most of them show an elastic behavior in a limited region where the stress and strain have a linear behavior. Elastic behavior of rubber-like materials under large deformations is known as hyperelasticity. These materials have a large elastic region with nonlinear relationship between stress and strain [8]. Linear elastic models do not accurately simulate the nonlinear behavior of hyperelastic materials; therefore, a special material model is needed. The motivation and developments in formulating the material models have discussed by Gent [9]. Rubber-like materials show hyperelastic behavior under static loads; while they show

viscoelasticity in dynamic mechanical load. Their behavior is fully related to the deformation speed. Elastomeric polyurethane enables fast, continuous and large deformations. These properties could guarantee protect of sensitive electrical parts.

Lee. S. J [10] has worked on analyzing the hyperelastic behavior of a composite material to design a shear actuator. In this work, a novel active material for controllable applications was designed and tested. The active material used is a lens shaped element to implement pure shear motion using gas pressure actuation. The lens elements were embedded in a polyurethane matrix. He tested the polyurethane elastomer in different test set-ups and derived their experimental data-set and then numerically analyzed them using Finite Element Method. The aim of the paper was to design the best lens shaped element to control shear deformation on the hyperelastic polyurethane. During the numerical analysis, the Ogden material model [11] was selected as the best model for impact test. The conclusion of the paper is: the lens element actuators approach a full circle when pressurized and causes shear deformation. Different hyperelastic material models are used to analyze deformation of the material due to shear stress. Schematic diagram of the system presented in Figure 2.1.

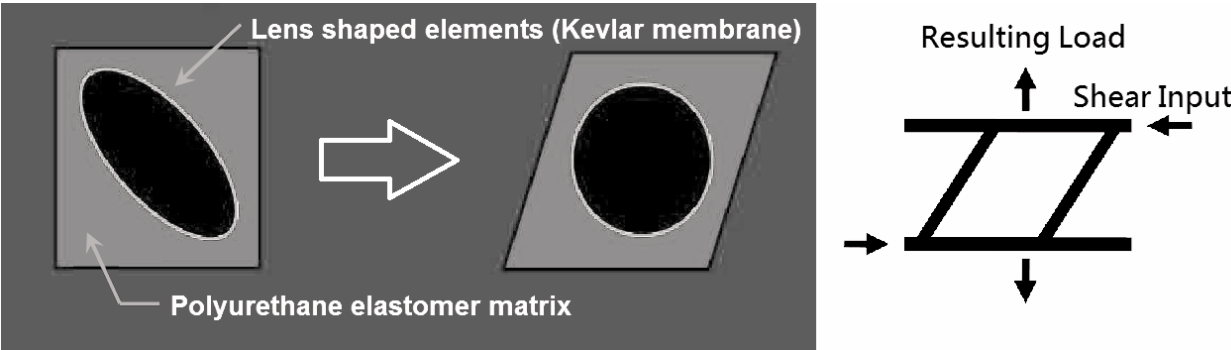


Figure 2.1. Schematic diagram of the behavior of the elastomer in simple shear [7]

In another work, Alsakraneh [13] presented the use of rubber buffer layer to protect embedded System-In-a-Package (SIP) device from high mechanical forces. The aim

of the paper is to reduce the transmitted stress to the embedded SIP device. The system was numerically analyzed the stress-strain on the embedded SIP using different testing conditions. Finally it is demonstrated that the strain on the SIP could decrease up to 84% with relatively thin layer of buffer material. Further, different variables such as the effect of thickness of rubber and epoxy, rubber brand and static force on minimizing the strain on the SIP were presented. The structure is presented in Figure 2.2.

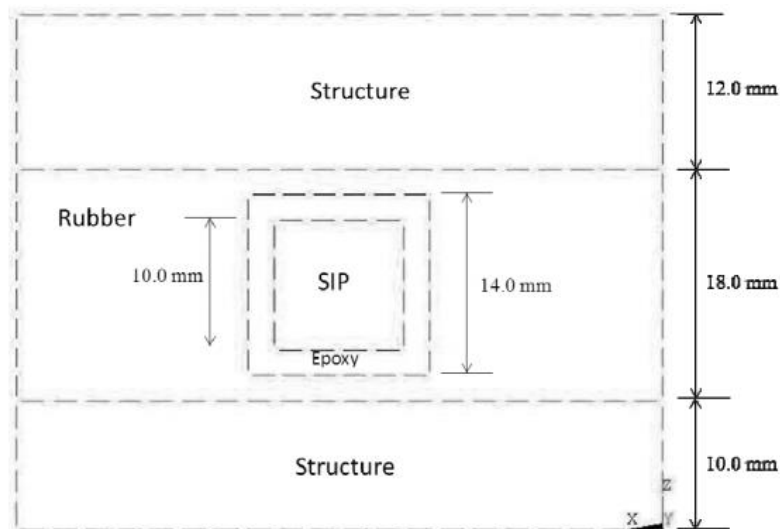


Figure 2.2. Middle cross section of entire structure [13]

Examples of using the hyperelastic behavior of rubber-like materials are presented above. Many researches performed on the viscoelastic behavior of the materials. The viscoelastic materials are particularly applicable to the protection of sensitive components from impact loads. They can be used as bumpers in automobiles, cushion in vibration systems, packaging, impact isolators and etc.

The numerical modeling of an electronic system embedded in multiple viscoelastic materials under impact loads was studied in [4]. According to the work, a design methodology defined for buffer layers which could significantly increase the protection of embedded electronic systems. The effect of thickness of different viscoelastic

materials on decreasing the stress on the electronic circuit was presented in the work. The author used a ball structure shown in Figure 2.3 which consists of different layers of viscoelastic materials.

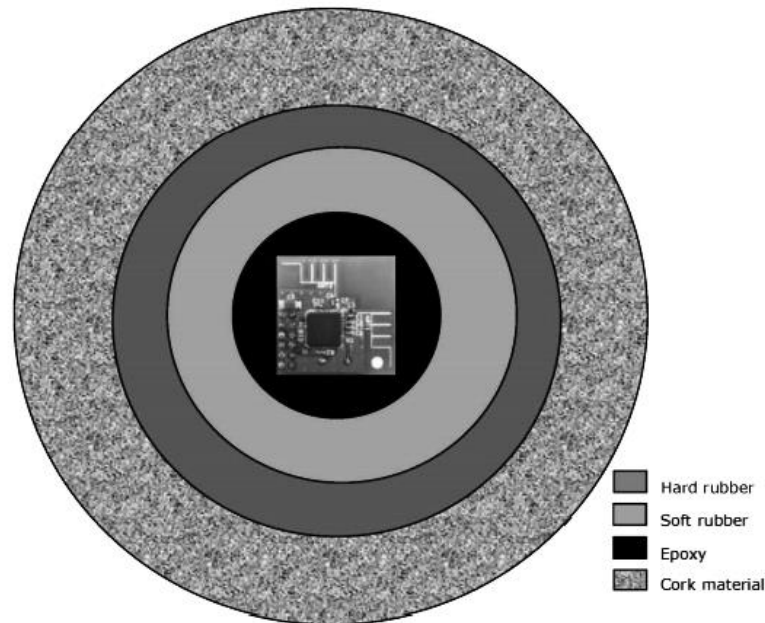


Figure 2.1. The multi-layered buffering system with embedded SIP [4]

In another work, dynamic model of polyurethane foam cushion is established [14]. The static compression testing and dynamic compression testing is performed on the material to build the nonlinear viscoelastic plastic deformation. Sung, D. K [5] modeled the nonlinear elastomer impact problem when a mass experience a collision with a contact pad which is mounted on the underlying linear dynamic structure. The viscoelastic contact pad modeled as linear and nonlinear stiffness and nonlinear contact damper. The underlying dynamic structure is calculated by Fourier spectral analyzer. The impact force used in this study developed when an ideal mass experiences a collision with the elastomeric contact pad. However the model does not include the specimen size or the dropped mass area and weight. The test structure is presented in Figure 2.4. The model analyzed just for special contact pad in specific test condition.

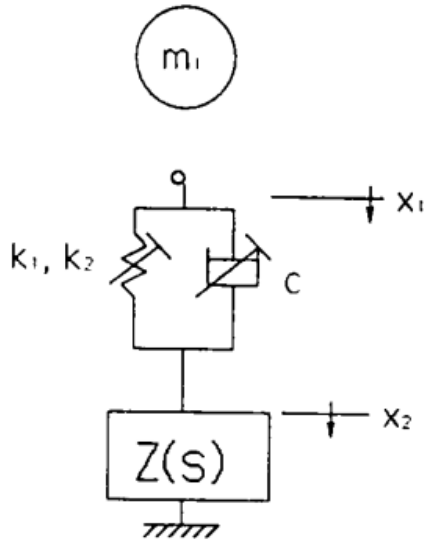


Figure 2.2. Nonlinear impact model [5]

We are trying to model the elastomeric contact pad in a way that the model includes the specimen size and testing conditions. For this purpose, the PD is modeled analytically by defining an analytic model and empirically using Neural Networks (NN). Then, PD is converted to the stress by using a derived differential equation. Further, the ANSYS software is used to numerically analyzing the stress on the specimen. ANSYS uses material models to simulate the material behavior. As mentioned before, linear isotropic material models could not accurately simulate behavior of hyperelastic materials. Then, nonlinear elastic material models are used. Each material model has a special Strain Energy Density (SED) function. There are many material models; however, in this study four material models are analyzed.

For numeric analysis of these materials, we first prepared the experimental data-set and then used them to evaluate different hyperelastic material models by using ANSYS. Experimental data of shear, uniaxial tension and biaxial tests are needed to obtain an acceptable Finite Element (FE) result. However, measurement of shear and biaxial tests require special mechanical devices. To compensate the lack of test setups, Valanis-Landen method is used to estimate the data-set of these tests. The FE implementation of specimens under uniaxial tension and pure shear tests is

evaluated using four separate material models in four different experimental data-set combinations.

In this study, data-sets of shear and biaxial tests are predicted from uniaxial tension and uniaxial compression tests which are mostly available in all laboratories. These data-sets are used to evaluate four different material models. Beomkeun Kim compared three different material models using experimental data-sets of Chloroprene Rubber [15]. According to the results; Ogden 3rd was shown to have a better convergence with the experimental data-sets, while Mooney-Rivlin and Neo-Hookean were not in an acceptable agreement range. However, the Gent model which is suitable for rubber modeling was not investigated. Jang *et al* worked on weatherstrip which is made of EMPM and TPE. However, he considered the combination of biaxial + uniaxial tension tests data-sets only to calculate the constants of material models [16].

2.2.1. Hyperelastic Material Models

As mentioned before, special material models are selected to define the nonlinear behavior of the material. The major difficulties of using FEM are: finding out the behavior of different material models, and determination of constants of relevant material model. In this thesis four material models are used to model the hyperelastic materials. These models are: Mooney-Rivlin, Ogden, Neo-Hookean and Gent. These material models have special SED functions. It should be noticed that, the constants of each material model and the constants of related SED functions are the same values.

SED functions are used for numerical modeling of the behavior of rubber-like materials. Constants of these SED functions are found using curve-fitting tool of ANSYS utilizing experimental data. To make a decent polynomial fit to the entire data-set and to find out the material model constants, data-set of multiple types of tests (uniaxial simple tension, planar shear and biaxial tension) are needed. Unfortunately, shear and biaxial tests need special test setups that are rarely found and expensive.

In order to compensate the lack of experimental data, known success of the VL function in characterizing the behavior of rubber-like materials is used. The effectiveness of the VL function in estimating the data-set of shear and biaxial tests from uniaxial tension and uniaxial compression tests has already been shown in [17-20]. This paper however presents a detailed description of numerical analysis of the hyperelastic materials utilizing experimental and estimated data-sets.

There are many approaches to estimate the experimental tests data-sets [17-20] and to analyze the hyperelastic material models [15-16] separately. However, to the best of our knowledge, numerical analysis of hyperelastic elastomers, based on predicted test results, has not been reported yet. Experimental set-up and estimation method is described in section (2.2.2).

2.2.1.1. Mooney-Rivlin

Mooney-Rivlin method is a hyperelastic material model introduced by Mooney and Rivlin which has options of 2, 3, 5 or 9-parameters. In general, increasing the order gives more accurate results. It is known that, material models having higher orders can be used for varied structural components of up to 200% deformation. Also, 2-parameter Mooney-Rivlin option is suitable for stains of up to 100% in tension and 30% in compression [21]. SED function of the material model is composed of linear combination of two invariants of the left Cauchy-Green deformation tensor as given below:

$$W(\bar{I}_1, \bar{I}_2) = C_{10}(\bar{I}_1 - 3) + C_{01}(\bar{I}_2 - 3) + \frac{1}{d}(j - 1)^2 \quad (1)$$

where, C_{10} and C_{01} are the material constants characterizing the deviatoric deformation of the material, \bar{I}_1 and \bar{I}_2 are the first and second deviatoric strain invariant, and d is the material incompressibility parameter. j is the determinant of the elastic deformation gradient which is equal to 1 for incompressible materials.

Therefore, for the last segment of the equation becomes zero [22].The general equation of SED function for infinite series is as follows:

$$W = \sum_{i,j=0}^{n \rightarrow \infty} C_{ij} (\bar{I}_1 - 3)^i (\bar{I}_2 - 3)^j \quad (2)$$

2.2.1.2. Ogden

An Ogden model is a hyperelastic material model. The SED function of this model is expressed by principal stretch ratios. Ogden model is proven to be a good hyperelastic constitutive model for large strains of incompressible materials [11]. The SED function of Ogden model is a special case of the VL function that has a capability of expanding experimental data-set of uniaxial tension to the other two test formats. It can be expressed as a nonlinear function of principle stretch ratios which is expressed as:

$$W(\lambda_1, \lambda_2, \lambda_3) = \sum_{r=1}^{n \rightarrow \infty} \frac{\mu_r}{\alpha_r} (\lambda_1^{\alpha_r} + \lambda_2^{\alpha_r} + \lambda_3^{\alpha_r} - 3) \quad (3)$$

where, λ_j ($j=1, 2, 3$), α_r , μ_r are the principal stretch ratios, and material constants respectively. Ogden model shows a good agreement with the experimental data even in high deformations of up to 700%, therefore; it is used most commonly to analyze the rubber-like components [21].

2.2.1.3. Neo-Hookean

This model uses the Hook's law which is applicable for materials having linear behavior at the first regime. A Neo-Hookean hyperelastic material model could analyze various structural components in small strains of up to 30% [21]. Mooney-Rivlin SED function is a series of powers which are usually truncated in the first term. Neo-Hookean model only depends on the first term of the Mooney- Rivlin SED function. Therefore, the SED function of this material model becomes:

$$W(\bar{I}_1) = C_{10}(\bar{I}_1 - 3) \quad (4)$$

the C_{10} constant could be expressed as:

$$C_{10} = \frac{\mu}{2} \quad (5)$$

where μ is the initial shear modulus [23].

2.2.1.4. Gent

The Gent model is a phenomenological model for hyperelastic materials which can be used to analyze the stress-strain behavior of isotropic incompressible hyperelastic materials. The Gent model, which is based on the theory of limiting chain extensibility, has a logarithmic SED function [24]. The SED function of the Gent model depends only on the first invariant (\bar{I}_1) of the left Cauchy-Green strain tensor, which is a logarithmic function of \bar{I}_1 and two material parameters μ and J_m which are initial shear modulus and limiting value of $\bar{I}_1 - 3$. SED function of the Gent model can be shown as:

$$W = -\frac{\mu J_m}{2} \text{Ln} \left(1 - \frac{\bar{I}_1 - 3}{J_m} \right) + \frac{1}{d} \left(\frac{J^2 - 1}{2} - \text{Ln}(J) \right) \quad (6)$$

where, d is the material incompressibility. Therefore, the last segment of the function tends to be zero.

For rubber-like materials, the relationship between the applied stress and the strain is fully nonlinear; therefore, the material models with nonlinear formula of SED function such as Ogden and Gent are expected to have better convergence with the experimental data set.

2.2.2. Experimental set-up

Two main experimental set-ups are used in this work to perform static and dynamic (impact) tests. The static tests are performed to define the constants of material models in order to use for numerical analysis of the material. The dynamic tests are performed to analyze the PD and stress during an impact.

As previously mentioned, Experimental results of only simple uniaxial tension test would not be sufficient. Therefore, finding the constants of a SED function (material model) requires adequate number of experimental data-sets. In this work, we use one practical (uniaxial tension), and two estimated (shear and biaxial) data-sets as an input. Due to lack of shear and biaxial test set-ups the results of these tests estimated using VL function. In order to explore the reliability of VL function, few shear tests are performed and the results are compared with the predicted shear test results. During the shear tests, the specimens fail around the clamp edges after about 120% of elongation. Therefore, the comparison can be done only for a range of limited strain. However, we could not make the biaxial tests due to the lack of experimental set-up in our laboratory.

During the static and dynamic tests, following conditions must be considered:

- Humidity and temperature dramatically affect the structural properties of the elastomers.
- High strain rate increases the damping force which consequently increases the value of stress-strain gradient and usually decreases the maximum endurable strain in simple tension test [8].
- According to the experimental experiences, the mechanical properties of the specimens saturate after about 30 days of manufacturing due to the vaporization.

By considering the arguments given above; all specimens should be manufactured and stored under the same conditions. Testing of hyperelastic materials should be performed in low strain rates (i.e. 5mm/min), and they should be tested after 30 days of manufacturing. Finally, if a test needs to be repeated; at least 30 minutes should be passed over the previous one due to the stress softening. When the rubber-like materials are deformed for the first time, their mechanical properties change. Therefore, after manufacturing the material, it should be stretched many times to saturate the mechanical properties before gathering data sets. This phenomenon is known as Mullins effect and the recovery time differs from material to material [25].

2.2.2.1. Details of the Material

The material used in this study is Vytaflex-10 which is a polyurethane elastomer with a shore hardness of A10, manufactured by Smooth-on. The material is commercially available in two separate containers that must be mixed in 1:1 proportions. The mechanical properties of Vytaflex-10 provided by the manufacturer are presented in Table 2.1. According to the manufacturer, a specimen can reach up to 1000% of elongation when tested 7 days after manufactured. However, due to the evaporation, the specimen reaches to its stable condition in 30 days and the maximum elongation decreases down to 800%.

Table 2.1. Mechanical properties of the V10 polyurethane elastomer

Material	Vytaflex-10
Shore A hardness [ASTM D-2240]	A10
Tensile strength [ASTM D-412]Mpa (psi)	1.37 (200)
Elongation at break [ASTM D-412] %	1000%
100% modulus [ASTM D-412]	25

Poisson's ratio	0.499
Density kg/m ³	990

2.2.2.2. Uniaxial Tension Test

Uniaxial tensile and compression tests are performed with a machine manufactured by U-test designed for uniaxial tests. For the tension test, the probe dimensions are selected in accordance with ASTM D-412 standard which is suitable for vulcanized rubber and thermoplastic elastomers. According to ASTM D-412, the specimen has to have a hollow dumbbell shape. The reason of manufacturing the specimens in dumbbell shape is to prevent the specimen failure at the clamps.

Uniaxial tension tests are performed on 20 specimens utilizing U-test machine. The variation of the test results about the mean are calculated to be around 10%. This variation could be mainly due to the small defects in the manufacturing process.

In this work, deformation only applies in one direction and the principal stretch ratio can be calculated using the equation given below:

$$\lambda_1 = \lambda = \frac{L}{L_0} = 1 + \varepsilon_u, \lambda_2 = \lambda_3 = \frac{1}{\sqrt{\lambda}} \quad (7)$$

where, λ_i ($i=1, 2, 3$), ε_u , λ , L, L_0 are principle stretch ratio, nominal tensile strain, stretch along uniaxial loading direction, gage length of the specimen during and before deformation respectively.

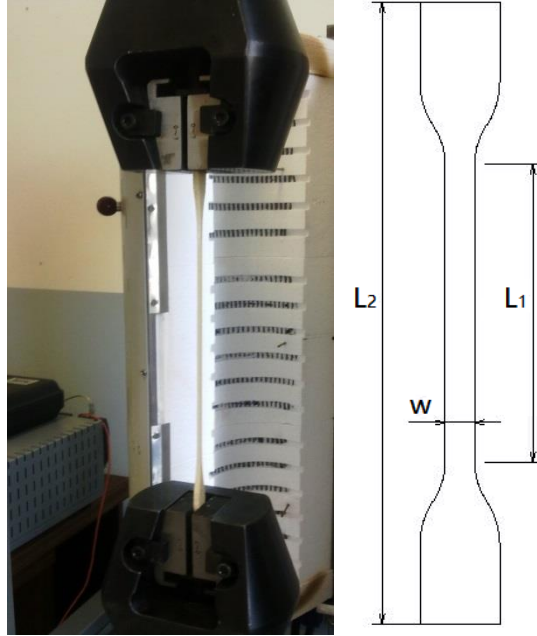


Figure 2.3. A photo of the uniaxial tension test machine during testing in approximately 300% of elongation (left) and the drawing of the specimen (right)

As shown in Figure 2.5, L_i ($i=1, 2$) is the length and W is the width of the specimen. In addition, engineering stress can be calculated by dividing the force measurements to the un-deformed cross-section area of the specimen. Principle stress states can be defined as:

$$\sigma_1 = \sigma = \frac{F}{A_0} = \sigma_2 = \sigma_3 = 0 \quad (8)$$

where, F , A_0 , σ_i ($i=1,2,3$) are the applied force, cross-sectional area and axial stress, respectively. According to Kearsley and Zapas, VL function can be calculated utilizing uniaxial tension and compression tests. [20] Following equation can be used to obtain $\dot{u}(\lambda)$ of the VL function:

$$\lim_{n \rightarrow \infty} \sum_{k=0}^{n-1} [t \left(\lambda^{(1/4)^k} \right) + t \left(\lambda^{-(1/2)(1/4)^k} \right)] = \lambda \dot{u}(\lambda) \quad (9)$$

where, t represents the true stress. According to this equation, there is an infinite number of true stresses and the first and the second terms are in opposite side of the un-deformed state ($\lambda = 1$). Therefore, both uniaxial tension and compression test results are needed to solve the equation for $\dot{u}(\lambda)$ of the desired points. The equation of the uniaxial engineering stresses can be written in terms of VL function as given below:

$$\sigma = \dot{u}(\lambda) - \lambda^{-(3/2)}\dot{u}(\lambda^{-(1/2)}) \quad (10)$$

2.2.2.3. Biaxial Test

Biaxial test requires special fixtures and high cost equipment, therefore; to minimize the total cost of the procedure and speed up the process, an alternative method should be used. For incompressible materials, uniaxial tension is equivalent to biaxial compression, uniaxial compression is equivalent to biaxial tension, and planar tension is equivalent to planar compression [8]. Biaxial test results can be estimated by using two methods; first, using an equivalent equation, and second, using a VL function. Using a simple mathematical conversion, biaxial stress-strain can be written as a function of uniaxial compression as follows:

$$\sigma_{biaxial} = -\sigma_{compressive}\lambda^{3/2} \quad (11)$$

In another approach, biaxial stress-strain relationship can be expressed in terms of VL function which can be given as:

$$\sigma_{biaxial} = \dot{u}(\lambda) - \frac{1}{\lambda^3}\dot{u}\left(\frac{1}{\lambda^2}\right) \quad (12)$$

where, λ represents the principle stretch ratio. Comparison of these two approaches is shown in Figure 2.6. According to the plot, both models generate almost the same results.

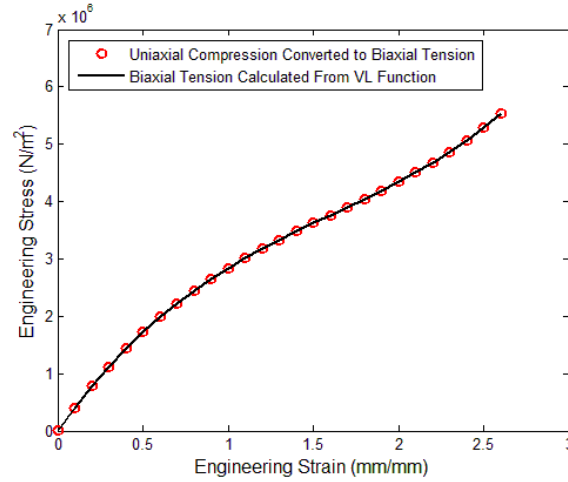


Figure 2.4. Estimated results of biaxial tension test using the equivalent equation and VL function

In uniaxial compression test, top and bottom surfaces of the specimen is lubricated in order to minimize the shear deformation. As shown in Figure 2.7, D and t represent the diameter and the thickness of the specimen which are 40 mm and 12 mm in dimensions respectively. Deformation and stress state of the uniaxial compression tests can be defined as:

$$\lambda_1 = \lambda = \frac{t}{t_0}, \lambda_2 = \lambda_3 = \frac{A}{A_0} \quad (13)$$

and

$$\sigma_1 = \sigma = \frac{F}{A_0}, \sigma_2 = \sigma_3 = 0 \quad (14)$$

respectively where, λ_i ($i=1,2,3$) is the principal stretch ratio and σ_i ($i=1,2,3$) is the axial stress.

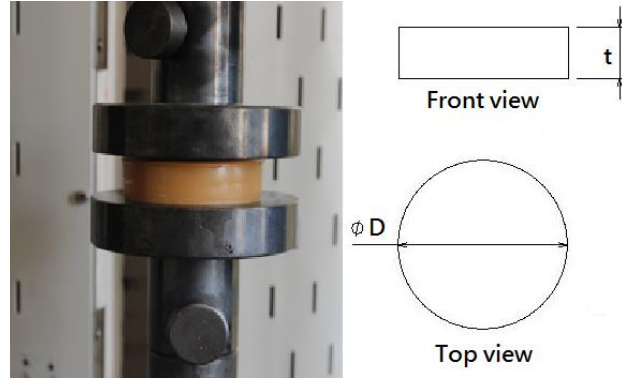


Figure 2.5. A photo of the uniaxial compression test (left) and the drawing of the specimen (right)

2.2.2.4. Shear Test

The stress state of the planar shear test is similar to the pure shear test. Shear test is also known as uniaxial tension test with a very wide specimen [26]. The most important feature of the specimen is that the width should be much larger than the direction of stretching to make thinning in thickness direction only. Experimental studies have shown that, the width of the specimen must be at least 10 times of the length. Only in this condition, the specimen is considered to be tested in the condition of the plane strain rather than the plain stress known as uniaxial tension test [11].

$$W \geq 10L \quad (15)$$

where, W and L represent the width and length of the specimen respectively. For the tests, we manufactured 5 specimens which are $200 \times 15 \times 0.9$ mm's in dimensions. During the tests, these specimens were all ruptured at the clamps after approximately 120% of deformation. Strain and stress states of planar shear test can respectively be defined as:

$$\lambda_1 = \lambda = \frac{L}{L_0}, \lambda_2 = 1, \lambda_3 = \lambda^{-1} \quad (16)$$

and

$$\sigma_1 = \sigma, \sigma_2 \neq 0, \sigma_3 = 0 \quad (17)$$

where, λ_i ($i=1,2,3$) and σ_i ($i=1,2,3$) represent principal stretch ratio and axial stress respectively. In addition, $i = 1, 2, 3$, corresponds to the length, width and thickness. Stress-strain relationship of the planar shear in the form of VL function can be expressed as:

$$\sigma_{shear} = \dot{u}(\lambda) - \frac{1}{\lambda^2} \dot{u}\left(\frac{1}{\lambda}\right) \quad (18)$$

Comparison of the VL function and the experimental test result of pure shear tests is shown in Figure 2.8.

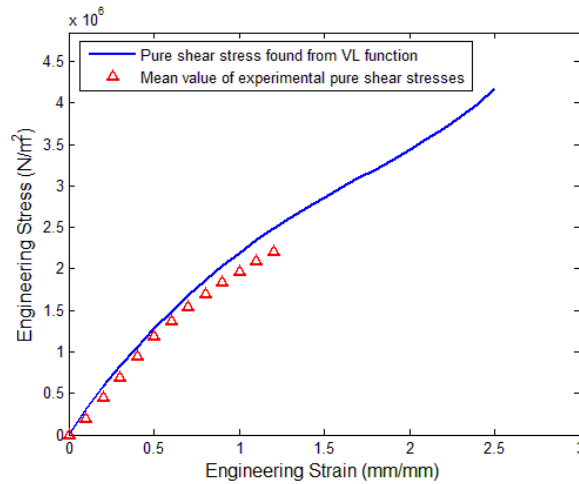


Figure 2.6. Comparison of pure shear test and corresponding VL function results.

2.2.2.5. Drop Test Device

In order to perform a dynamic compression test, a test device is designed (Figure 2.9) similar to [27]. The mass and the height of the impact rig are adjustable. The minimum mass of the impact rig is 1.866 kg and can be increased by adding mass. Specimens having a top area of up to 254 cm² can be tested in the setup. All specimens are manufactured by pouring the elastomer in cylindrical molds made of Plexiglas. The accelerometer used in this study is 3256A1 manufactured by Dytran which detects shocks of up to 300 g and working frequency range of 1 to 10 KHz.

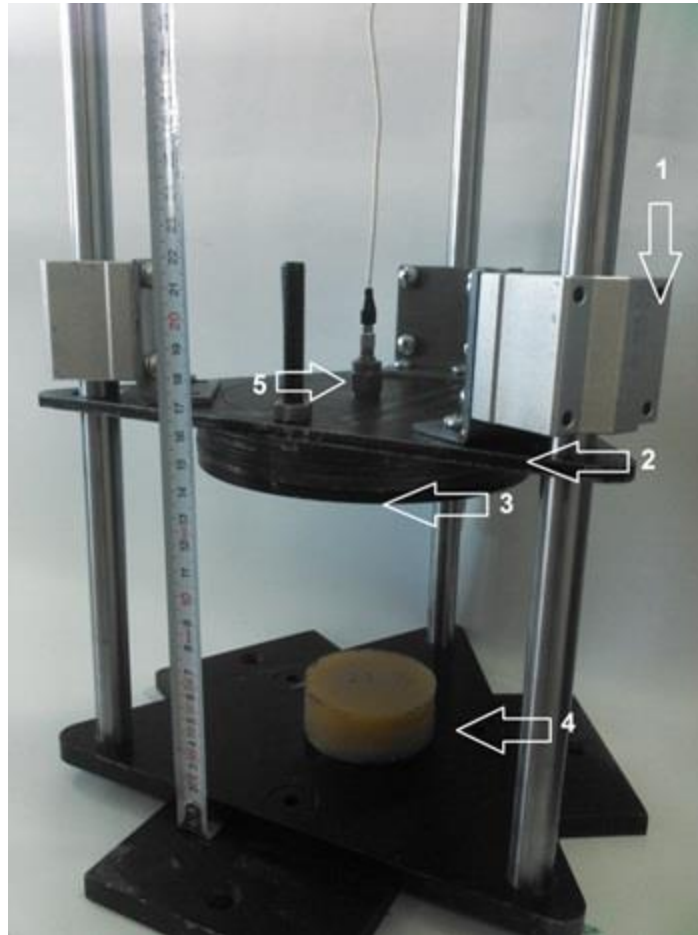


Figure 2.7. A photo of the designed drop test; cylindrical bearing (1), impact rig (2), adjustable mass (3), Specimen (4), and accelerometer (5)

Deceleration data of the collision is measured by the accelerometer and transferred to data acquisition card via a signal conditioner. LABVIEW software is used to record the data. A sample test result of the specimen with an area of 28.26 cm^2 , a thickness of 5.19 mm , a drop height of 5 cm and a drop mass of 1.866 kg is shown in Figure 2.10. As seen in this figure (vertical upward direction is positive), there are many local PDs, however, only the first PD wave is considered for modeling due to its highest value. The subsequent peaks of decelerations are caused by rebounding of the impact rig. Other tests were performed for drop heights of between 5 to 60 cm (or velocities from 1 to 2.62 m/s) and drop masses of between 1.866 to 4.363 kg . In this study, seven specimens with constant thicknesses and varying areas between 3.14 to 200.96 cm^2 ;

nine specimens with constant areas and varying thicknesses from 3.7 to 27 mm are tested. To model the material behavior 16 specimens are manufactured and tested; specimens presented in Table 2.2.

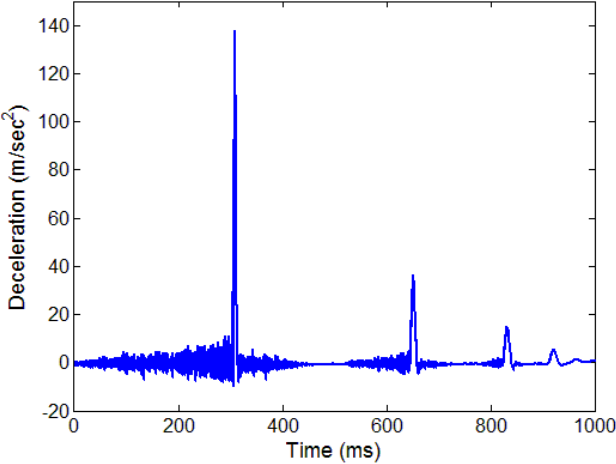


Figure 2.8. A sample plot of the impact deceleration of a specimen, where; A=28.26 cm², T=5.19 mm, M=1.866 kg and H= 5 cm versus time

Table 2.3 presents the results of some experiments made in this work. Note that the experiments given in Table 2.3 are a very small portion of the whole tests done in this work.

Table 2.2. Specimens manufactured for testing

Area 28.26 Cm ²	The specimen number								
	Thickness (mm)								
	1	2	3	4	5	6	7	8	9
	3.7	5.2	7.75	8.33	10.88	11.63	16.7	22.3	27

Thickness 8.5 mm	The specimen number							
	Area (cm ²)							
	10	11	12	13	14	15	16	
	3.14	12.56	28.26	50.24	78.5	113	153.8	

Table 2.3. Sample variables and PD results of specimens

Target variable	Area A (cm ²)	Thickness T (mm)	Drop height H (cm)	Drop mass M (kg)	Average peak deceleration (g)
Thickness T	28.26	5.19	5	1.866	138.26
			10		182.15
			15		255.75
		16.7	5	1.866	25.75
			15		79.38
			25		141.1
Drop height H	28.26	11.63	5	1.866	32.25
			15		108.85
			25		197.75
			35		294.98
Area A	12.56	8.3	5	1.866	41.3
			15		109.06
			25		192.12
	78.5		5	1.866	105.91
			10		203.65
			15		245.65
Drop mass M	28.26	11.63	15	1.866	109.01
				2.479	91.11
				2.965	83.41
				3.431	79.23
				3.897	78.93

Each test is repeated four times under the same conditions and the average PD values are presented here only. The PD may increase when the tests are repeated while keeping the other parameters constant due to the viscoelastic relaxation of the material. This phenomenon could be eliminated by waiting for a while depending on the material type between the tests [28].

Using table 2.3, following conclusions can be drawn: The PD increases with increasing drop height and area and decreases with increasing thickness and mass individually, when the other constants are kept constant.

2.3. Manufacturing Process

In this thesis, we tried to find a method to manufacture a rugged robot. For this purpose, a unique manufacturing method called Shape Deposition Manufacturing (SDM) is used. As it comes from its name, this method includes shaping and deposition in order to manufacture desired models. The rugged robot must endure external impacts. Vulnerable components of the robot must be embedded in a host object which reduces the impact force considerably. There are some materials that satisfy this mechanical property. In the next section, properties of the host material are going to be explained which covers the robot. In this section, manufacturing process of the SDM is described in detail.

2.3.1. Shape Deposition Manufacturing (SDM)

This manufacturing method enables us to manufacture mechanical 4 bars linkages monolithically without needing a screw and a bolt. One of the properties that make SDM interesting is its repetitive material addition, and material removal that allow making models layer by layer with desired thicknesses. This property enables to manufacture 3-D shapes that conclude making design more simple and monolithic. Other feature that makes it more interesting is embedding mechanical and electrical components between the materials. It can be anything like a motor, spring or a wire and etc. Figure 2.11 presents the process of SDM:

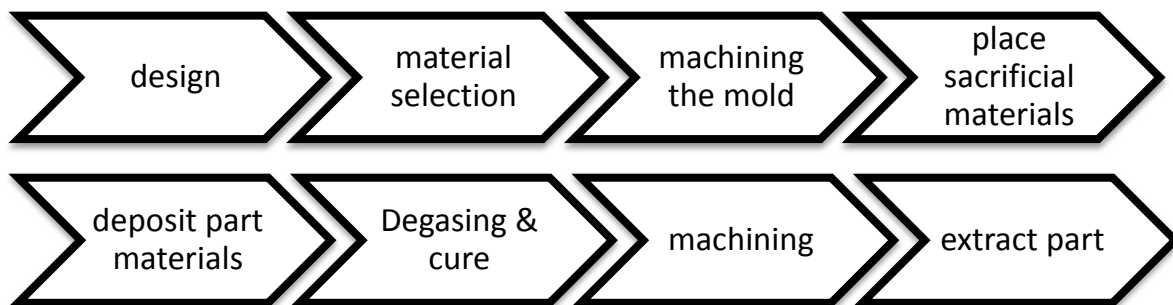


Figure 2.9. The manufacturing process of the SDM

In order to embed components and manufacture different 3-D shapes, it is required to make repetitive cycle as it is shown in Figure 2.12.

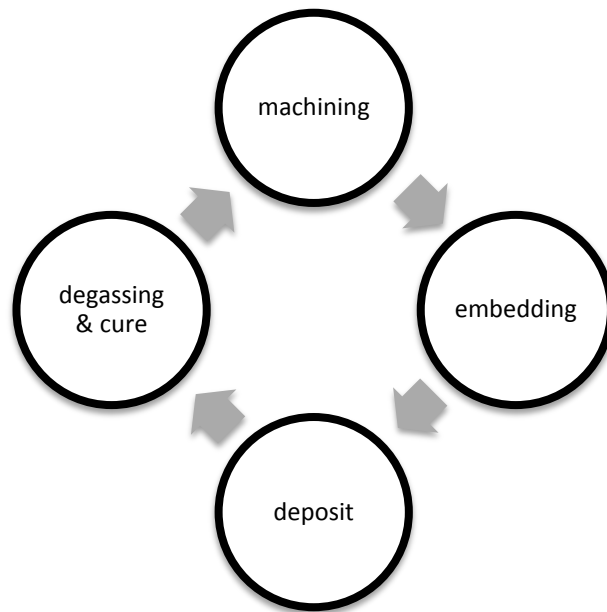


Figure 2.10. The SDM cyclic process involving material addition and removal and component embedding

This method needs a mold (made of gypsum or wax), pour-able materials (for example polyurethane elastomer), material for making it easy to extract poured material from mold (for example Vernik or Glycerol) and if requires, embedding components. The mold and the part material are machined using the same method, typically a CNC mill. It should be noticed that some of the materials are not machine-able. The mold uses a sacrificial material. This means that the mold can be used again or ejected after being used. The polyurethane which is known as part material will be pour after the machining the mold [26-27].

2.3.2. CAD Model Creation

Using CATIA as a CAD would enable us to design desired models. However, important issue is the general strategies considered to build order.

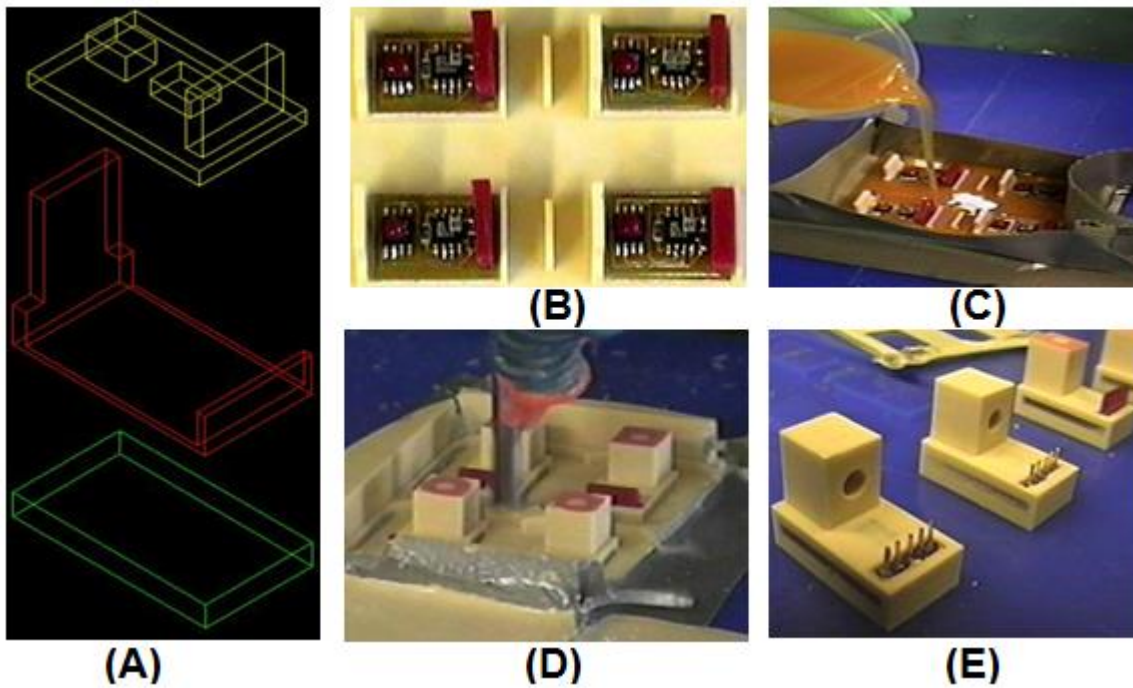


Figure 2.11. An example of SDM manufacturing process: Designing (A), Embedding process after machining the mold (B), Depositing the part material (C), Machining (D), and Releasing from mold (E). [29]

The embedded components are designed, selected and prepared for embedding. This process involves the fixtures, machining the part and sacrificial material and even pre-assemblies. It is important to notice the tolerances of mold. Applying proper fixtures for the embedded components depend on considering appropriate tolerances in design process.

2.3.3. Materials in SDM

The materials involved in SDM are classified into 5 categories: part material, support material, temporary material, sacrificial material (dam material) and embedded components.

2.3.3.1. Part material

Polyurethane, rubbers, elastomers, ceramics and metals can be used as the part material in SDM [30-31]. In this work, the part material is chosen among polyurethane elastomers. Selection of the part material needs some consideration factors such as;

- Shore hardness
- Shrinkage
- Chemical stability
- Gel time
- Machinability
- Viscosity
- Curing time

In some models like flexible joints, two different materials are required. In this condition, binding, gel time and chemical reaction between two materials must be tested. Table 2.4 presents some of polyurethane elastomers with different mechanical properties.

Table 2.4. Examples of mechanical properties of elastomeric polyurethanes

Hardness (shore A)	Cost tl/kg	Company	Tensile psi	Cure time hour	Elongation	Specific gravity gr/cm ³	Gel time min
18	171	C3	140	24	150%	1.25	20
24	428	C3	140	24	150%	1.25	20
34	130	C3	140	24	150%	1.25	20
40	81	C3	140	24	150%	1.25	20
50	149	C3	140	24	150%	1.25	20
60	73	C3	140	24	150%	1.25	20
87	330	C3	140	24	150%	1.25	20
20	100	vyta flex	200	16	1000%	1	30
40	100	vyta flex	522	16	660%	1.02	30
60	100	vyta flex	880	16	480%	1.04	60
33	30	Era	290	18	435%	1.2	N/A
83	30	Era	551	18	450%	1.08	N/A

95	30	Era	1885	18	375%	1.13	N/A
75 shore D	40	Era	6526	22	N/A	1.19	N/A

2.3.3.2. Support Material

The support material is typically chosen from different waxes but we decided to use gypsum as a support material. A proper candidate for the support material should have high chemical stability, good machinability, low shrinkage, and ease to remove from the part. All of these properties can be found in gypsum. Gypsum has perfect chemical stability, machinability, no shrinkage and could be easily removed from the mold.

2.3.3.3. Temporary Material

The temporary material is used to make an internal geometry such as bearing houses or tube connectors. The typical temporary materials are water solvable or low melting point waxes. Some chemicals such as PEG can be very easily dissolved in water. Various chemical solutions have also been used to be dissolved in special types of polymers. It should be easily removed or dissolved after the manufacturing process to create the internal void in the part assembly. The temporary material is especially useful for embedding mobile components where the joint should have a certain clearance.

2.3.3.4. Sacrificial Material

Sacrificial material is known as dam material. It is used as a dam during casting to hold the liquid state polymer material. It is usual to use modeling clay to build the dam walls; however, other materials also can be used. It should be removed before urethane is machined. The clay and its usage is shown in Figure 2.14; the yellow material is the temporary material which is used for making internal voids.

2.3.3.5. Embedded Components

As previously mentioned, one of the abilities of SDM is embedding the components

between part materials. During the designing, it should be noticed that;

- Robust binding: components should have a robust binding with the part materials;
- There are some problems like weak bonding of soft and hard polyurethane because of bubbling and chemical reaction between two materials.
- Embedded components should not be damaged in the machining process.
- The components should keep required clearance from the part material where a free motion is required.
- Shrinkage must be considered.

It is important to minimize the bubbling using various techniques such as pre-vacuuming the material before molding or molding in vacuum environment, and improving the surface finish of the embedded components. The typical embedded components include motors, pistons, air cylinders, chips, and strain gage sensors. A collection of embedded components are shown in Figure 2.13 [29].



Figure 2.12. Sacrificial material (yellow), support material (blue) and embedded components [29]

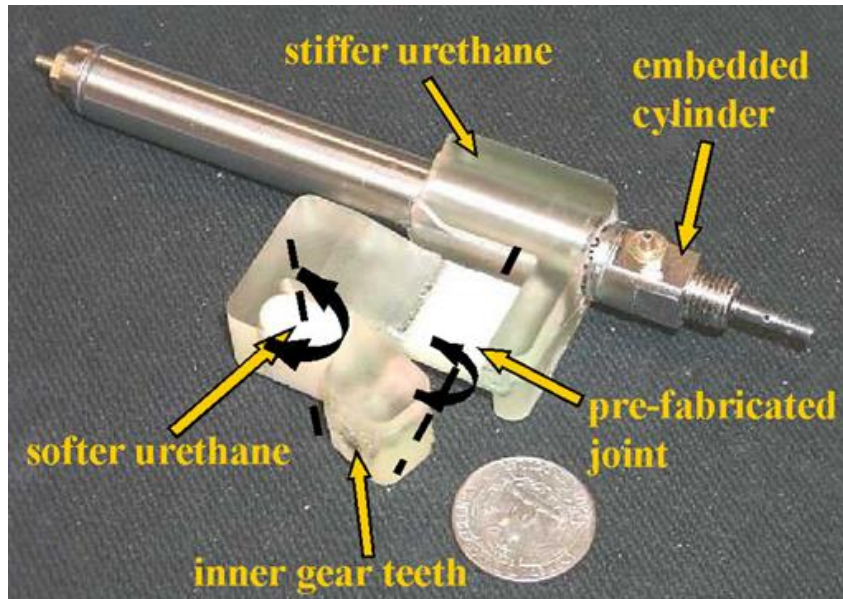


Figure 2.13. Example of embedded components Double-Jointed compliant leg (fabricated by SDM) [29]

2.3.3.6. General Considerations in Material Selection

In selecting the part material general considerations are:

- Low cost
- Long shelf-lives, long pot-lives, low toxicity
- Strong layer to layer binding
- Ability to pour even in low temperatures
- Material shrinkage should be minimized for the dimensional accuracy of the SDM process
- Part materials should exhibit good machinability
- Good mechanical properties and chemical stability for part material
- Part materials should solidify without the formation of internal voids
- Part and support materials should have physical properties such as low viscosity and good machinability that favor the process control of SDM
- Part and support materials must be physically and chemically compatible
- Part material should be easily taken out of the support material after the

molding process completed

- Good binding strength between soft and hard polymeric materials.

other considerations specified for biomimetic robot fabrication;

- Good inter layer shear strength between the embedded components and the surrounding polymer material
- Good binding property between polymeric materials and metals (e.g. embedded components)
- The temporary material should be easy to remove in order to make internal cavities such as pistons
- The embedded sensors, tubes and actuators should lead to minimum trapped air in the polymer material after casting.

By considering the notes above; we decided to use Vytaflex polyurethane with different shore hardness. The Era and C3 companies were not selected because they need special manufacturing process like pre-heating the mold before molding and curing in specific temperature. Polyurethane which is used as a part material is shown in Figure 2.16. It consists of two materials (resin and hardener) which has a mixing ratio of 1:1.

Interaction between materials plays an important role in bonding and embedding of different component in materials. Understanding the chemical reaction in combination of two materials, strength of binding, flexibility of the joints and considering the feasibility of connections are important factors which should be considered. For example, it is difficult to connect soft material to hard material because they do not machine very well. For solving this problem, orderly manufacturing methodology is used. For example, deposit hard polyurethane first and then machine it for making cavities to deposit the soft material.



Figure 2.14. Polyurethane used as a part material

2.3.3.7. Effective Parameters on Changing Mechanical Properties of Elastomers

These parameters could change the mechanical properties:

- Cure time
- Mixing time
- Annealing
- Creep
- Degassing
- Stress softening (Mullins effect)

Each effect is described below in detail.

2.3.3.7.1. Cure time

After molding the polyurethane, it takes 1 day to fully cure and ready to take it out from the mold. As time passes, the gasses in the specimen vaporizes and it's color gets darker. At the same time, its mechanical properties such as stiffness (K), damping coefficient (C), and maximum stress and strain durability change. The results are presented in section 3.

2.3.3.7.2. Mixing time

Polyurethane elastomers are manufactured by mixing two liquid in one by one ratio for four minutes. In short mixing time polyurethane chains will not have enough chance to bond well and this generates a negative effect on mechanical properties of polymer.

2.3.3.7.3. Annealing

In order to obtain ultimate dynamic properties of a polyurethane elastomer, the material need to be annealed. Most effective temperature for annealing is generally just below the melting point (T_m) of the material. Mechanical properties such as resilience and flexibility in low temperature can be improved by annealing as well. These improvements occur because of reduction in the amount of interphase between the hard and soft block domains. Since the interphase is the mixture of hard and soft block domains, the material able to rearrange and/or separate, becoming either part of an increasingly well-structured hard phase or an amorphous soft phase as shown in Figure 2.17. The annealing is performed using the device shown in Figure 2.18.

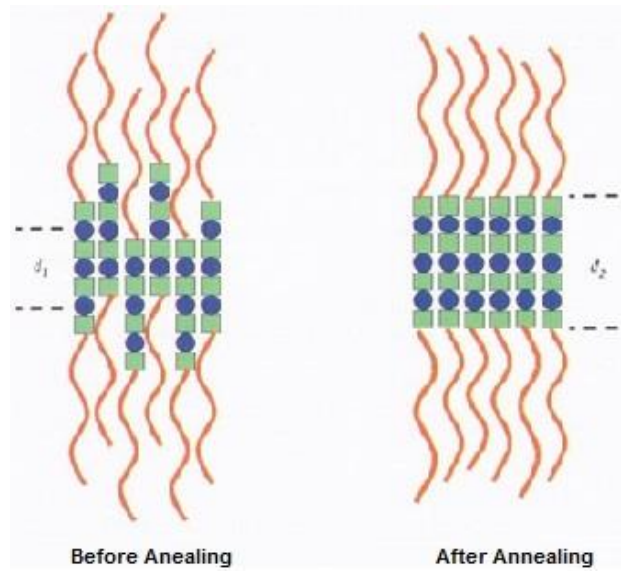


Figure 2.15. Effect of annealing on arrangement of domains [32]



Figure 2.16. Annealing device

2.3.3.7.4. Creep

Creep in polymers happens in every temperature. Creep rate (velocity of creep) increases by increasing temperature and stress.

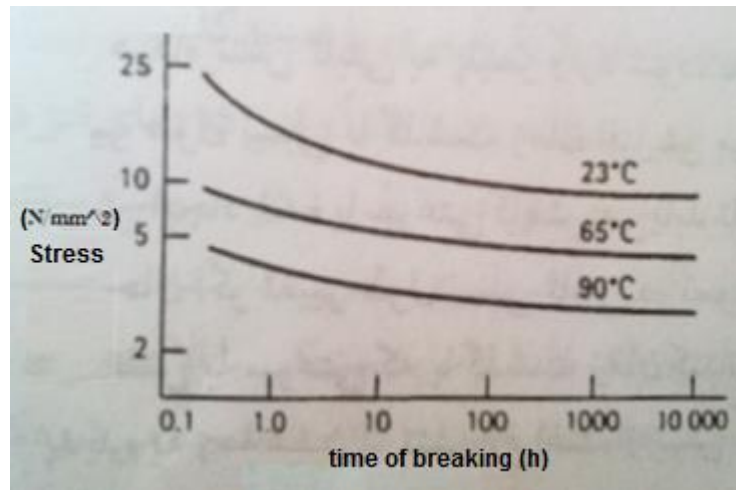


Figure 2.17. Creep effect [32]

2.3.3.7.5. Stress softening (Mullins effect)

Under repeated tensile strain, most of the polymers exhibit a reduction in stress after the initial extension; this phenomenon is known as the Mullins Effect [16]. The Mullins effect is “Phenomenon observed in rubber-like materials where the equilibrium stress-strain response softens with the strain history”. The Mullins effect has these features:

- The cycled material has a more compliant response at strains smaller than the previous maximum strain
- When the Mullins effect occurs, the microstructure breaks down with increasing deformation, and the initial structure cannot rebuilt

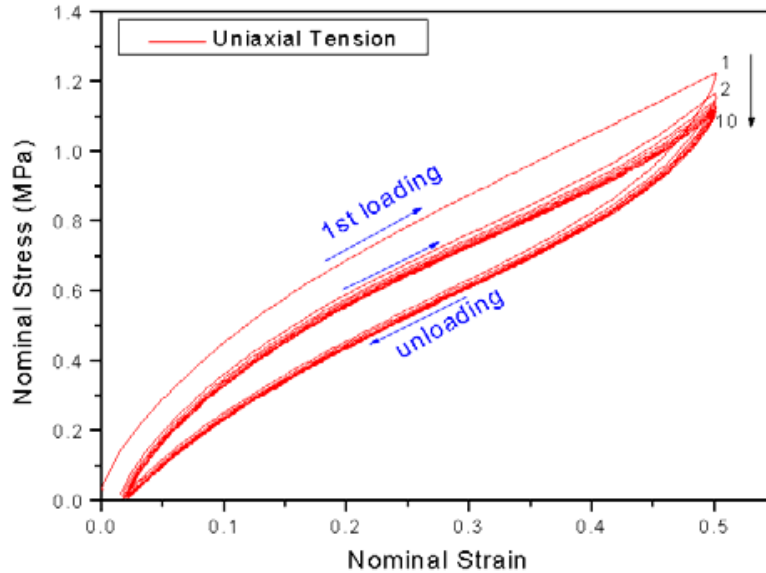


Figure 2.18. Mullins effect [16]

2.3.4. Different Manufacturing Process of SDM

The SDM process includes two main manufacturing processes; the material addition and removal. Each of these two processes is subdivided into bulk (uncontrolled) and selective (controlled) methods.

Selective deposition means controlled material addition. In this process, the materials are deposited into a designed geometry using a special 3-D rapid prototyping machine. The selective material deposition requires Fused Material Deposition (FDM) or stereo lithography which are expensive.

Bulk deposition process known as uncontrolled material addition. In this case material is free to fill the mold. Example of this type is explained before in figure 2.14. After the molded material is completely cured, the material gets ready for machining. Removing the undesired parts from the material is known as selective removal.

Selective removal is the controlled material removing process. The undesired sections of models are removed using a CNC.

Bulk removal is uncontrolled material removal. Hot water jet, melting, chemical etching are example of this method. Whole sacrificial material is removed in bulk removal method; consequently this method is not very accurate. Four main manufacturing process of SDM is described in detail in Appendix 1. Furthermore, an example of manufacturing a spring-loaded hinge is presented in Appendix 2.

3.3.5. Fixturing Challenges for Flexible Components

Embedding flexible components in the part material is very challenging issue because; the flexible components do not keep its shape constant in designed place without fixtures. To solve this problem, three main methods are described:

Fluid adhesive fixture method: This method is not very accurate. This is a simple and valid method when the required positioning accuracy is not very tight and it is not need to be in tension. However, it is a rather unreliable skill-dependent method since performance consistency cannot be expected.

Pre-encapsulation: This method describes pre-embed flexible component in a polymer. Having a layer of polymer, the flexible component keeps safe from chemical reactions. Embedded components should have sufficient rigidity and density to keep its shape and displacement by flotation. This method has less spatial limitations during embedding process and also fixture can be removed from the component before its incorporation into the mechanism in production. The best way to define geometry of a flexible component is to apply tension. For example fiber reinforcement elastomers can be produced by holding fibers under tension condition by using anchors and string alignment nut placed in the mold under tension condition and pouring polymer to encapsulate fibers. The pre-encapsulation fixture is described in Appendix 3.

Suspending fixture method: This method is used to create a specific harness for flexible components to keep their shape in cavity. The harness keeps flexible components in three or more locations. These multiple securing parts would be in one rigid piece until poured polymer fully got rigid. For releasing polymers from cavity top part of the support block removed by CNC. Since flexible polymers can be damaged in this method and complexity of designing the support block, it is not very common method. The pre-encapsulation method is proper for simple geometries and also it can be applied in small sizes as well. But this method has its own advantages like enabling to achieve more complex geometries. The suspending fixture is presented in Appendix 4.

3. RESULTS AND DISCUSSIONS

3.1. Operations on Material

Effective parameters on mechanical properties of elastomeric materials are described in previous section. In this section, results of some of these operations are presented. As mentioned before the mechanical properties of elastomeric materials could change over time. This happens because of vaporization of chemical gasses trapped in the material. Temperature and humidity have large effects on vaporization of the gasses; therefore, all specimens are stored in room conditions. Figure 3.1 shows elongation at break over time. Five specimens are manufactured and tested each day under the same conditions.

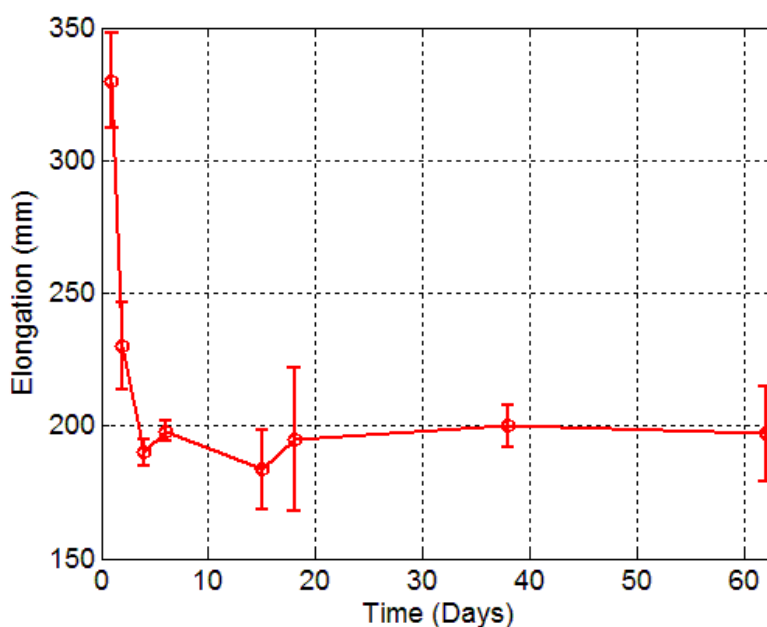


Figure 3.1. Plot of elongation vs. time (days)

As it is seen in the plot, the elongation decreases rapidly in the first days but the graph saturates after 30 days. As it seen in Figure 3.1, the specimens tested in day 19 have large errors mainly due to the manufacturing problems. The maximum force

that specimen endures during uniaxial tension test is shown in Figure 3.2. It should be noticed that the width and the length of the specimens are kept constant. .

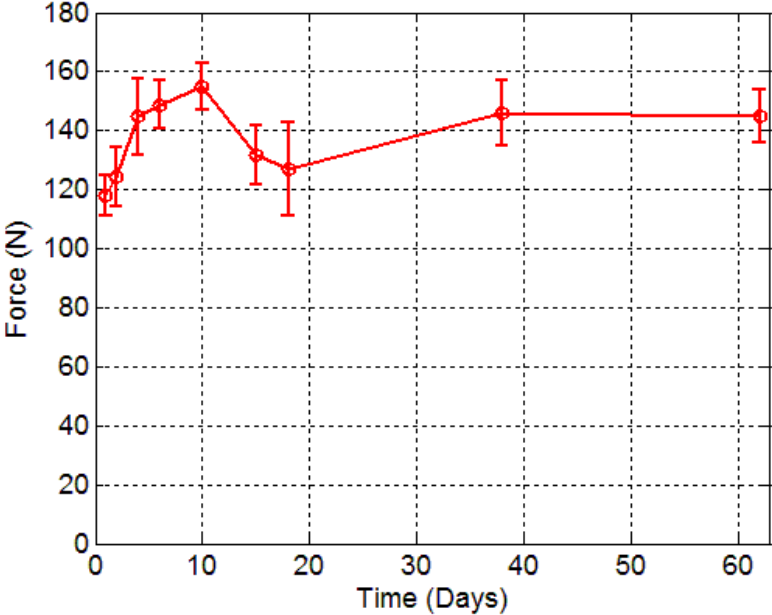


Figure 3.2. Plot of load/thickness vs. time (days)

As previously mentioned, the polyurethane elastomer is made by mixing two materials (resin and hardener). According to manufacturer the elastomer should be mixed for three minutes. We have found that mixing time below three minutes dramatically decreases the maximum endurable stress of the material. Further, the annealing could be applied to the material by heat the specimen to 150°F (65°C) for 4 to 8 hours after overnight cure; the maximum endurable stress increases up to 30% however the maximum strain decreases 5%.

3.2. Increasing SDM Performance

Conventional SDM process uses flat surfaces as contact surfaces each layer; however, we have found that increasing the cross section of bonding would increase the maximum bonding between layers. For this purpose, we manufactured and tested

different cross sectional bonding. Different cross sections and the results of uniaxial tension are presented in Table 3.1. Example of two different materials bonded is presented in Figure 3.3.

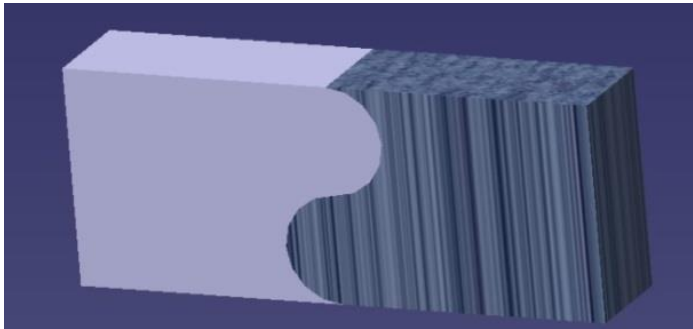
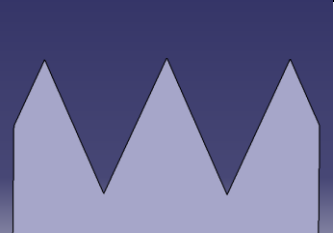
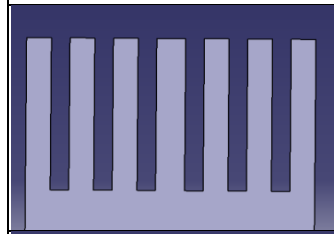
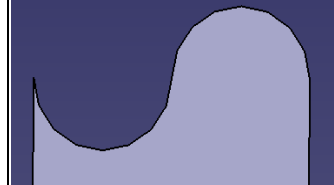
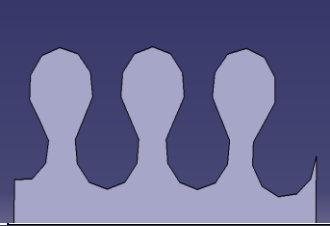
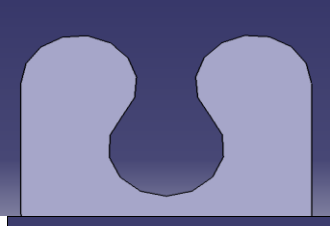
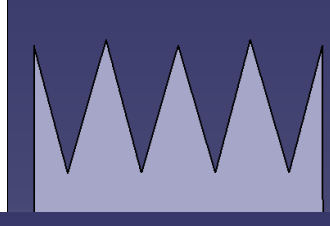
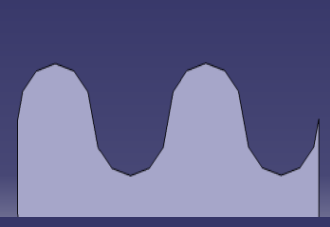



Figure 3.3. Bonding of two different materials

Table 3.1. Tension test on specimens with different contact area

Bonding type	Average of maximum force(N)	Average of thickness (mm)	Force(N)/ thickness (mm)
	735	7.38	99.5
	652	7.7	84.6
	647	6.1	106

	562	7.4	75.9
	441	7.3	60.4
	646	6.1	105.9
	702	7.2	97.5
	650	7.4	87.8

3.3. Finding constants of Hyperelastic Materials

3.3.1. Constants of Mooney-Rivlin

Constants of SED function having 2 and 9-parameters of Mooney-Rivlin models derived from using the experimental uniaxial tension test and two estimated shear and biaxial test results are listed in Table 3.2.

Table 3.2. 2 and 9-parameter Mooney-Rivlin constants

Constants	Mooney-Rivlin options	
	2-parameter	9-parameter
C10	4.5383E5	2.8203E5
C01	42559	2.422E5
C20		14067
C11		-12031
C02		-4124
C30		-1104
C21		1538.6
C12		44.44
C03		-5.748

3.3.2. Constants of Ogden

Constants of the hyperelastic material model according to the experimental uniaxial tension test and two estimated shear and biaxial test results are calculated as:

$$\mu_1=1.2313E+006$$

$$\alpha_r=1.8068$$

3.3.3. Constants of Neo-Hookean

According to the experimental uniaxial tension test and two estimated shear and biaxial test results, the constant of the Ogden material model is calculated as [23]:

$$C_{10}=1.0322E6$$

3.3.4. Constants of Gent

Constants of this hyperelastic material model utilizing uniaxial tension test and two estimated shear and biaxial test results are calculated as:

$$\mu_m = 1.0322e6$$

$$J_m = -1.7989e12$$

3.4. Results of FEA

Numerical analysis is applied to the specimen under uniaxial tension and pure shear using ANSYS. Four material models (Mooney-Rivlin, Ogden, Neo-Hookean, Gent) were numerically tested in four test combinations (uniaxial tension + biaxial, uniaxial tension+ shear, shear + biaxial, uniaxial tension + Shear + Biaxial) using Experimental data-set of uniaxial tension, and two estimated data-set of shear and biaxial tests.

The work started by developing a FE model using ANSYS 11. The element type was selected as solid 20node186 for meshing the specimen; the element has quadratic displacement behavior and characterized by 20nodes having three degrees of freedom on each node: translations in the nodal x, y, z directions. Moreover, because of its large deformation capabilities, it is used for meshing hyperelastic materials. Constants of the SED function of the selected material model were calculated using ANSYS curve fitting tool. As boundary conditions; one end of the specimen is fixed and the displacement is applied to the other end. The detailed algorithm of the numerical analysis of hyperelastic materials using ANSYS is described as a block diagram as given in Figure 3.4.

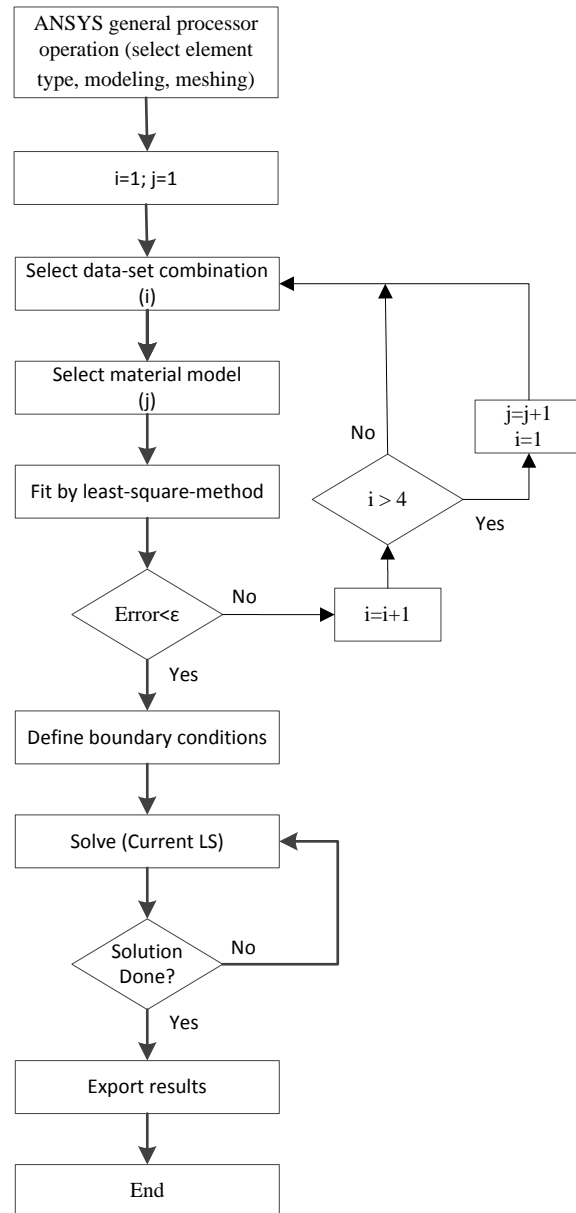


Figure 3.4. The block diagram of ANSYS analysis

3.4.1. Data-set Combination Effect on Different Material Models in Uniaxial Tension Test

In this section, comparison of numerical analysis of a specimen under uniaxial tension test using different inputted data-sets combinations are considered. For this purpose, four material models were evaluated and the results were presented in Figure 3.5-3.8. As shown in these figures, combination of uniaxial tension + biaxial and biaxial +

shear data-sets presented the best and worst results respectively, in all material models. As shown in Figure 3.5 Mooney-Rivlin cannot numerically solve the problem for large strains using the combination of uniaxial tension + shear or biaxial + shear data-sets.

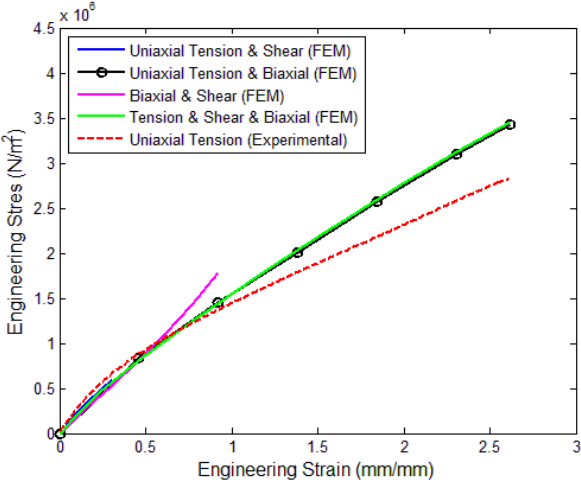


Figure 3.5. FEA of the uniaxial tension test using Mooney-Rivlin (9-parameter) model

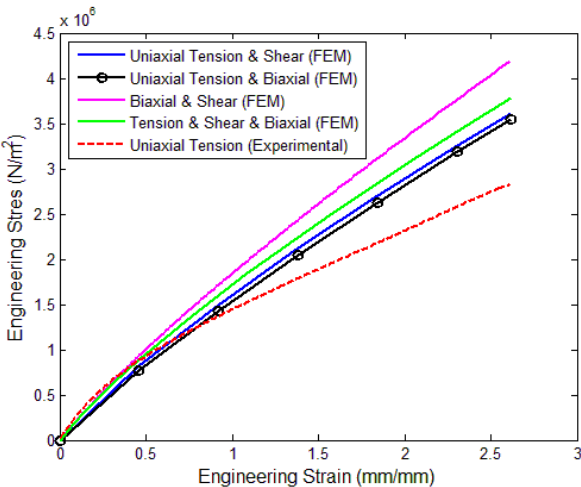


Figure 3.6. FEA of the uniaxial tension test using Ogden 1rd model

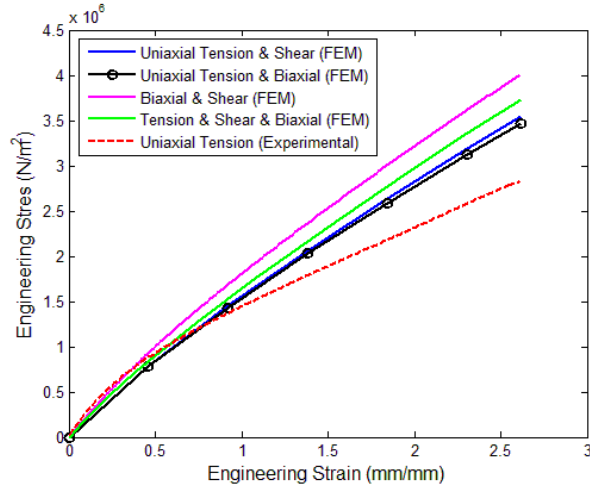


Figure 3.7. FEA of the uniaxial tension test using Neo-Hookean model

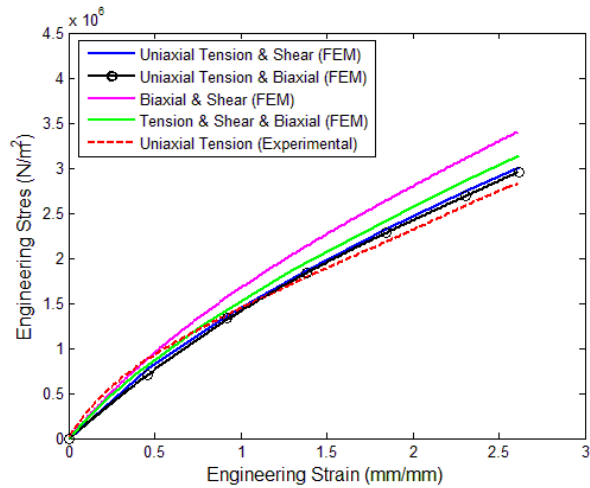


Figure 19. FEA of the uniaxial tension test using Gent model

3.4.2. Data-set Combination Effect on Different Material Models in Shear Test

In this section, numerical analysis of the specimen under pure shear test was performed using different data-sets combinations and material models. As shown in Figure. 3.9-3.12, biaxial + shear data-sets combination presented the best convergence in all material models. Moreover, Mooney-Rivlin could solve the model

using biaxial + shear data-sets combination only. In addition, Ogden model could not solve the model using combination of all three types of test data-sets.

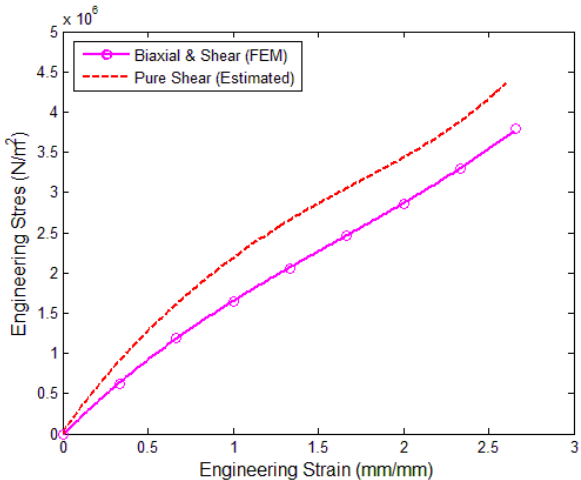


Figure 3.9. FEA of the pure shear test using Mooney-Rivlin (9-parameter) model

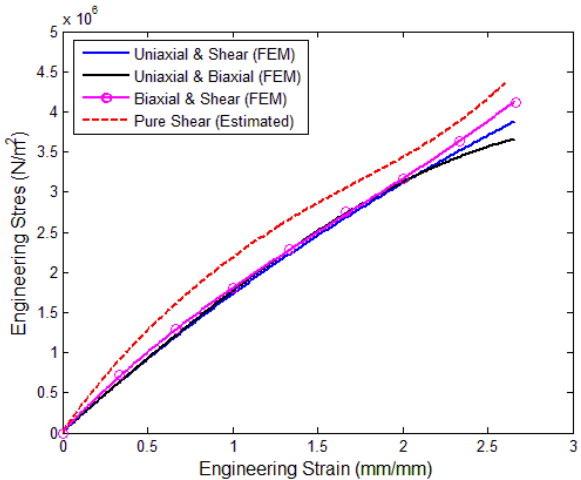


Figure 3.10. FEA of the pure shear test using Ogden (1-rd) model

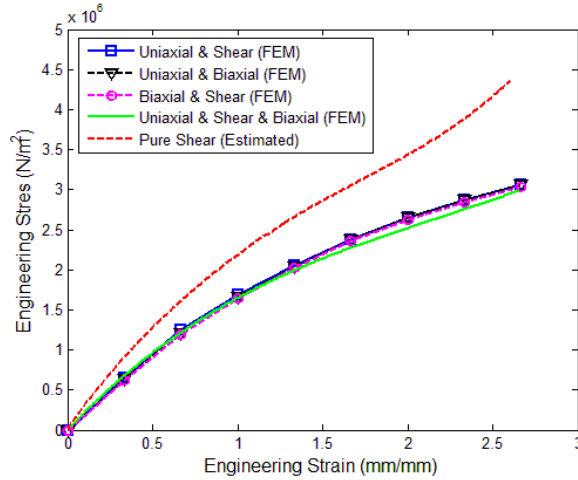


Figure 3.11. FEA of the pure shear test using Gent model

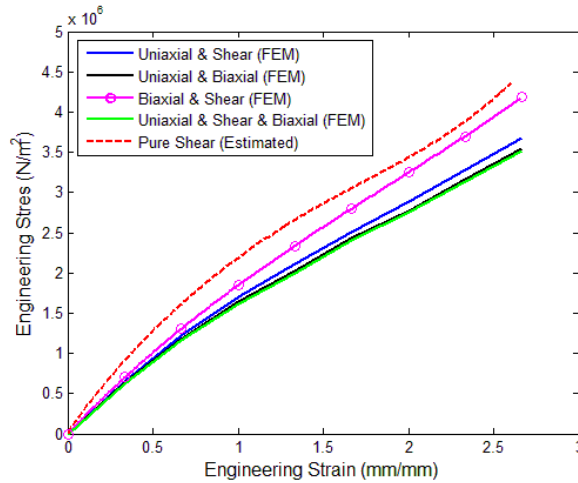


Figure 3.12. FEA of the pure shear test using Neo-Hookean model

3.5. Comparing Different Material Model Results

The best combination of inputted data-sets for uniaxial tension and pure shear test was found in the previous section. In this section, the best data-sets combination of each model is compared.

Figure 3.13 shows the comparison of aforementioned material models, using uniaxial tension + biaxial data-sets combination which is proven to be the best combination in previous section for uniaxial tension. In order to study the effects of orders in material models, 2-parameter Mooney-Rivlin is also evaluated. As shown in Figure 3.13, 9-parameter Mooney-Rivlin is more precise than 2-parameter model. However, none of

them are in good compliance with the experimental data-set. It is shown that the Gent model has the best convergence.

Figure 3.14 shows the comparison of different material models using combination of biaxial + shear data-sets which was already proven to be the best combination for pure shear test in the previous section. Neo-Hookean model demonstrates the best convergence with the estimated pure shear test.

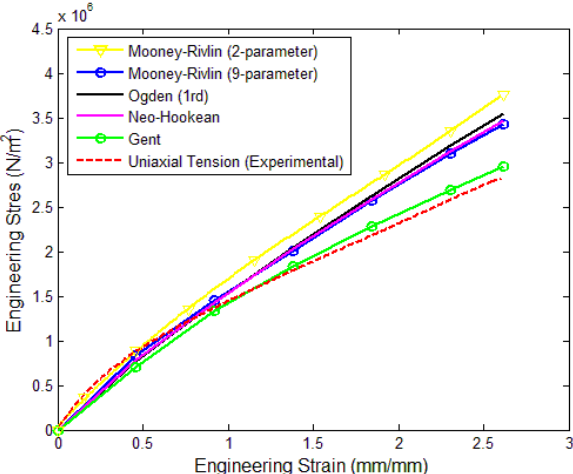


Figure 3.13. Difference of material models in analyzing uniaxial tension test

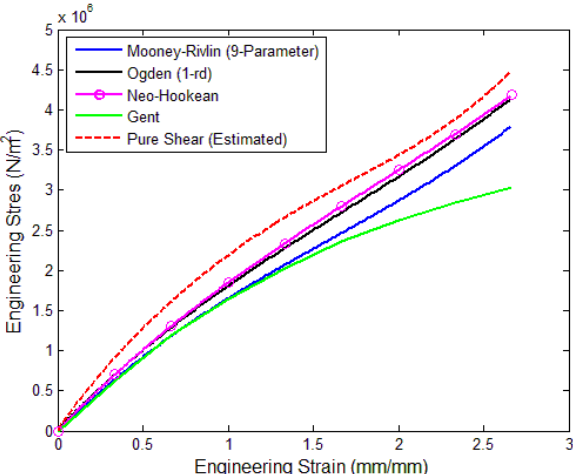


Figure 3.14. Difference of material models in analyzing shear test

To compare FE results with the experimental results, the average Root-Mean-Square (RMS) error was utilized for different strain intervals. The average RMS error can be calculated as:

$$\text{Average RMS error} = \frac{1}{M} \sqrt{\sum_{i=1}^N \left| \frac{\sigma_{exp} - \sigma_{FE}}{\sigma_{exp}} \right|^2} \quad (19)$$

where, M is the number of points at which the stress is calculated by FE Analysis, σ_{exp} is the stress of experimental data and σ_{FE} is the stress calculated from FE analysis. Results are presented in table 3.3. This Table shows the average RMS error of different material models calculated for analyzing uniaxial tension and pure shear tests.

Table 3.3. RMS error of material models for each test models

Uniaxial tension test					
	Mooney-Rivlin 9-parameter	Mooney-Rivlin 2-parameter	Ogden 1-rd	Neo-Hookean	Gent
RMS $0 < \epsilon < 1$	0.160	0.166	0.198	0.192	0.25
RMS $1 < \epsilon < 2$	0.191	0.226	0.201	0.193	0.104
RMS $1 < \epsilon < 2.5$	0.306	0.367	0.335	0.316	0.117
RMS $0 < \epsilon < 2.5$	0.1466	0.1883	0.162	0.1542	0.100
Pure shear test					
	Mooney-Rivlin 9-parameter	Ogden 1-rd	Neo-Hookean	Gent	
RMS $0 < \epsilon < 1$	0.380	0.320	0.318	0.381	
RMS $1 < \epsilon < 2$	0.273	0.213	0.201	0.281	
RMS $1 < \epsilon < 2.5$	0.239	0.164	0.143	0.284	
RMS $0 < \epsilon < 2.5$	0.164	0.128	0.121	0.182	

3.6. Impact Modeling

In this work, we developed an analytical and empirical models of a peak deceleration (PD) using the results of experimental drop tests. In the analytical model; thickness, area, drop mass and drop height are considered as separate functions. In the empirical model; Neural Network (NN) is used. Further, stresses on the materials are calculated using differential equation and Finite Element Method (FEM). Finally, all methods are compared and the best approaches are found.

Mechatronic applications are increasing exponentially and taking over the pure mechanisms recently. However, these applications utilize cameras, sensors, actuators and etc. which are sensitive to applied acceleration and stress. Therefore, many mechatronics devices cannot be used in many real-world applications. In this work, we focused on the ways of minimizing acceleration and stress by embedding the electronic devices in a host object made by rubber-like materials; which are widely used in minimizing the intensity of impact loads or accelerations. Polyurethane elastomers are viscoelastic rubber-like materials with very wide shore hardness which provide different dynamic properties. They can be used as bumpers in automobiles, cushion in vibration systems, packaging material, impact isolators and etc.

Since, the aim of this study is to protect the vulnerable components of a mechatronics device from elevated accelerations; in this study we developed an analytical and empirical (using Neural Networks) model of PD. These models could predict the PD of hypothetical specimens under different impact loadings. To the best of our knowledge, there has not been any work done to model the PD on variable specimen size and testing conditions. In both analytical and empirical models; the area, thickness, collision velocity (drop height) and collision mass are considered as separable functions. The stress in the material is also analyzed both analytically using a differential equation by converting PD to the stress and numerically using FEM. Finally, these models are compared to each other.

In this study, the elastomeric contact pad (specimen) is assumed to be the cover body of the robot experiencing the collision which is mimicked by a test device

manufactured in this work. This work continues with the details of the experimental set-up, modeling of the PD, stress analysis, discussion and conclusion.

3.6.1. Modeling of PD

3.6.1.1. Analytical Model of PD

The analytical model of deceleration proposed in this work considers area, thickness, drop height and drop mass as variables and assumes that these parameters are not functions of each other's.

$$PD = A(a) \times T(t) \times H(h) \times M(m) \tag{20}$$

where, A, T, H and M are functions of area, thickness, drop height and drop mass respectively.

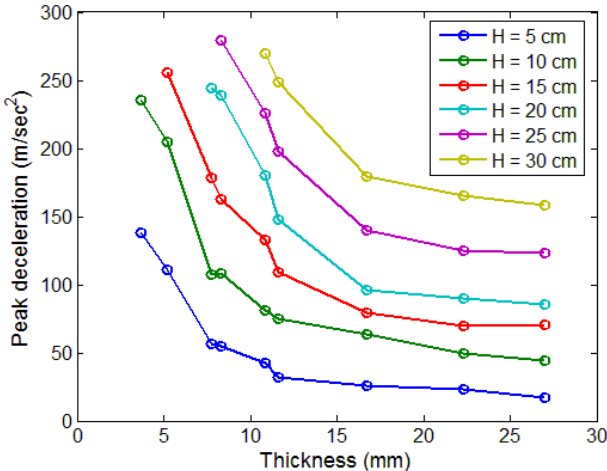


Figure 3.14. An example plot of PD vs. thickness with different drop height

Figure 3.15 shows the experimental results of deceleration of specimens with different thicknesses for different drop heights. According to the results, deceleration trends look similar for different drop heights keeping the area and drop mass constant but changing the thickness. Utilizing the plot; thickness of 8.33 mm, area of 28.26 cm²

and drop mass of 1.866 kg are chosen as reference points. The coefficient of thickness is found utilizing a best fit by keeping all parameters fixed but changing the thickness with a reference point of 8.33 mm. The coefficients of area and drop mass can be found similarly as well. The area function is calculated at an area of 28.26 cm² as the reference point where thickness, drop height and mass are constants and fixed to 8.5 mm, 15 cm and 1.866 kg respectively. The mass function is calculated at a mass of 1.866 kg as the reference point where thickness, area and drop height are constants and fixed to 8.33 mm, 28.26 cm², 15 cm respectively. In this work, all the test results are best fitted at an arbitrarily chosen drop height of 15 cm using MATLAB. The coefficients can be calculated using the best fit curves given below;

$$T(t) = 2.7 \exp(-0.157t) + 16.77e^{-2} \exp(28.03 \times 10^{-3}t) \quad (21)$$

$$A(a) = 3.295 \exp(-3.93/\sqrt[5]{a^2}) \quad (22)$$

$$M(m) = 3.07 \exp(-1.159m) + 60.84e^{-2} \exp(32.71 \times 10^{-2}m) \quad (23)$$

where, t (mm), a (cm²), m (kg) are the variables of thickness, area and mass respectively.

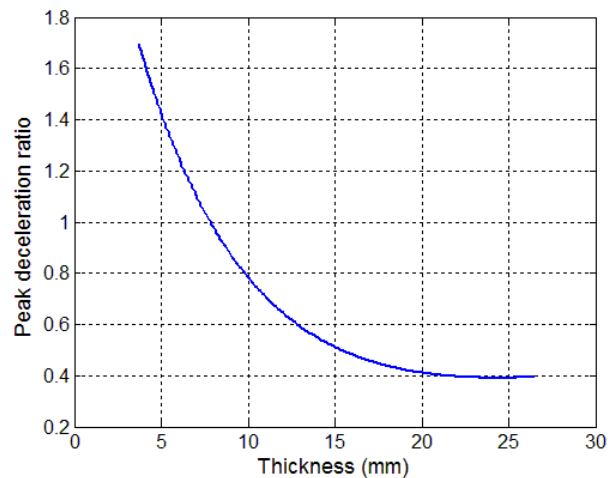


Figure 3.15. A best fit plot of deceleration ratio vs. thickness

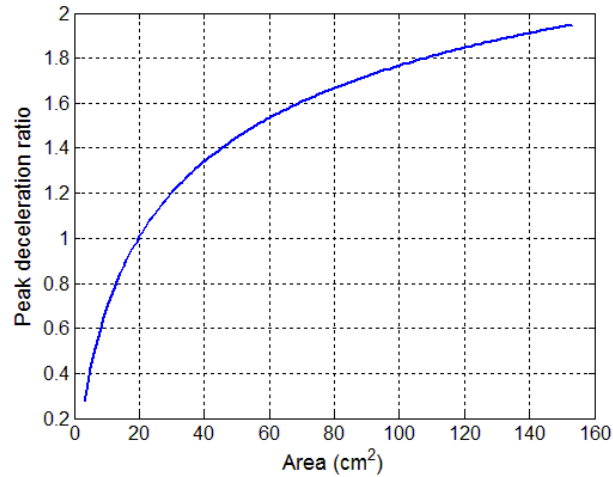


Figure 3.1620. A best fit plot of deceleration ratio vs. Area

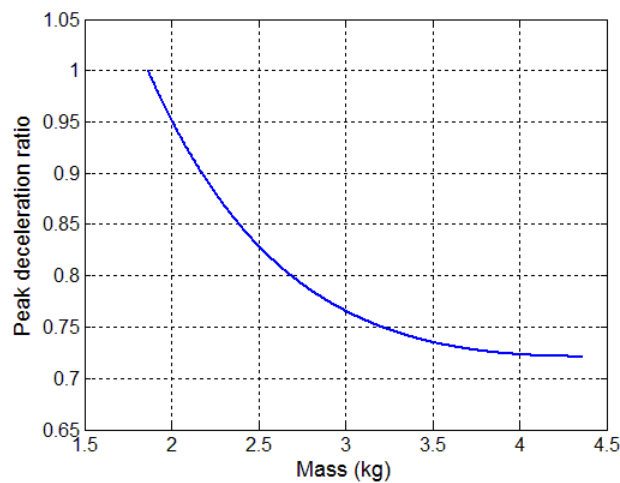


Figure 21. A best fit plot of deceleration ratio vs. mass

Although thickness, area and mass are converted into dimensionless number, the function of drop height is left with a unit of g (m/sec^2). This function is modeled up to 35 cm height due to accelerometer limitations where the reference specimen's area, thickness and drop mass are constants and fixed to 28.26 cm^2 , 8.33 mm and 1.866 kg respectively.

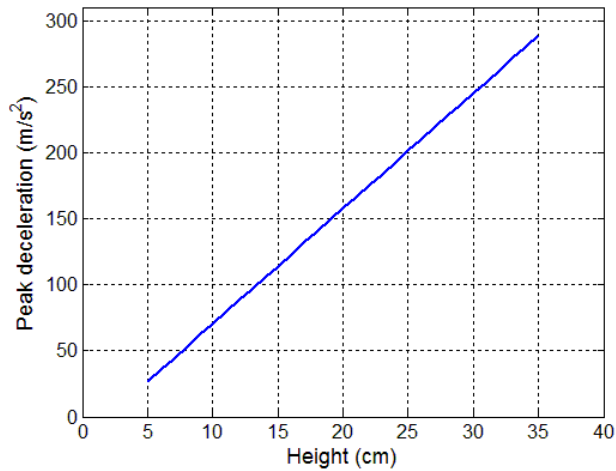


Figure 228. A best fit plot of PD vs. height

The best fit of the drop height function is;

$$H(h) = 8.722h - 16.67 \quad (24)$$

where, h is the drop height of the impact rig. Using the coefficients of each parameter and the drop height function, PD of any V10 specimen can be predicted.

3.6.1.2. Empirical Modeling (NN method)

In the previous section, the effect of four parameters including, area, thickness, drop weight, and drop height is modelled analytically. However, in this section the NN is applied to the experimental data. Designed NN could predict the PD of any combination of the four parameters. The perceptron algorithm is implemented for this problem. Two kinds of perceptron algorithms are compared in this work. One of them has two layers and the other has one layer. It is seen that the two-layer perceptron have smaller Minimum Squared Error (MSE). Then, the two-layer perceptron is decided to be used.

Tansig and Purelin transfer functions are used for the first and second layer, respectively. The designed NN uses Levenberg-Marquardt algorithm as the instruction function of training. Input data are divided randomly to the three sets which are as follows: 70% for training, 15% for validating and 15% used for testing. The regression analysis of different data-set using multilayer perceptron (MLP) implemented in this work is shown in Figure 3.20. The regression analysis verifies the suitability of the designed MLP [33]. Figure 3.21 shows the performance diagram of the selected algorithm. The MSE of validation graph has a descending trend and the indicated circle shows the best point for training the algorithm. The overall NN structure is provided in table 3.4. The number of neurons in each layer is determined by trial and error.

Table 3.4. The artificial NN structure

Structure	Multilayer perceptron
Number of hidden layers	2
Number of neurons on each hidden layers	First layer: 5; Second layer: 4
Hidden layers activation function	Purelin, Tansig
Number of training sample	2569
Learning method	Levenberg-Marquardt algorithm

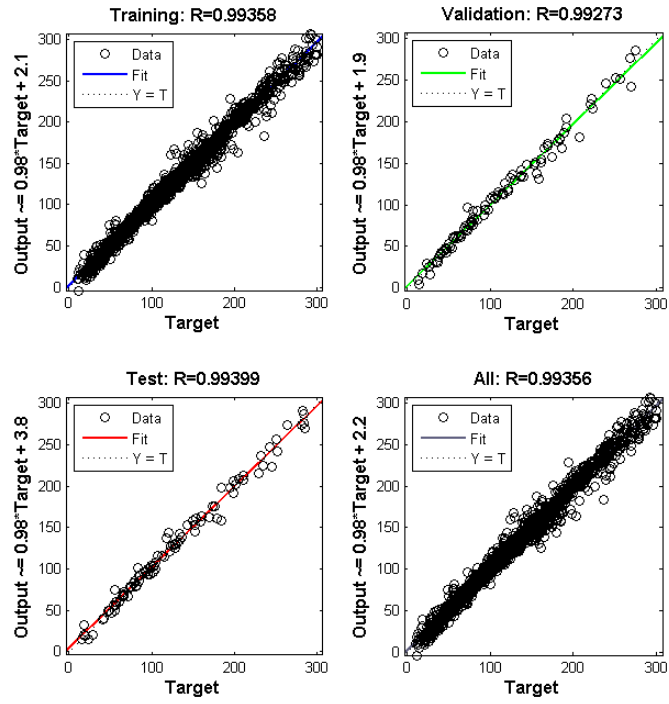


Figure 3.19. Regression analysis of MPL network.

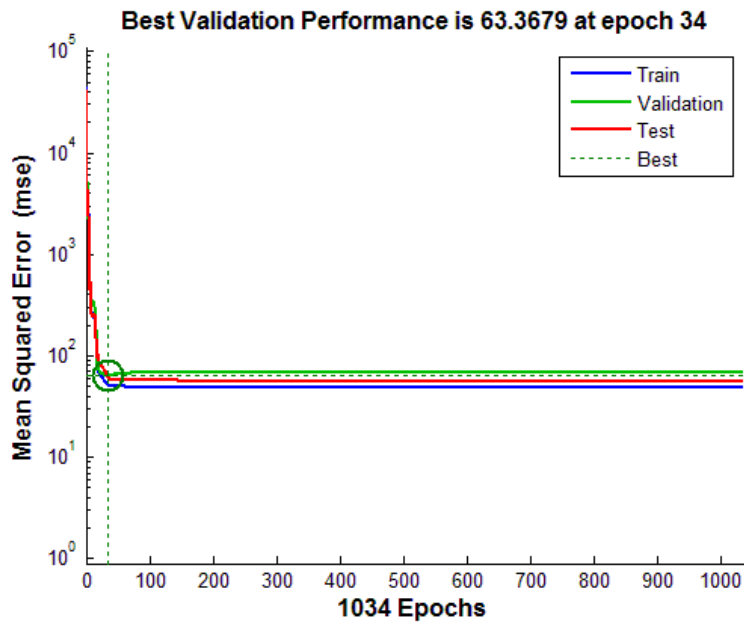


Figure 230. Performance of the NN.

3.6.1.3. Comparison of Analytical and Empirical Modeling

Some specimens are manufactured to analyze the accuracy of the analytical and empirical models. Table 3.5 represents the specimen size and testing conditions of these specimens. To compare the analytical and empirical results with the experimental results, the average Root-Mean-Square (RMS) error is utilized. The average RMS error can be calculated as:

$$\text{Average RMS error} = \frac{1}{M} \sqrt{\sum_{i=1}^N \left| \frac{PD_{exp} - PD_{model}}{PD_{exp}} \right|^2} \quad (25)$$

where, M is the number of points at which the PD is calculated analytically or empirically, PD_{exp} is the result of experimental data and PD_{model} is calculated via analytical or empirical analysis. Results are presented in table 3.6.

Table 3.5. Specimens manufactured for testing

specimen	No. 1	No. 2	No. 3	No. 4	No. 5
Area (cm ²)	16	12.56	8	19.26	9.07
Thickness (mm)	16.5	8.3	9.6	11.5	40
Drop mass (kg)	2.479	1.866	4.363	3.431	2.965
Drop height (cm)	57	5	27	13	40

Table 3.6. RMS error of each model

specimen	No. 1	No. 2	No. 3	No. 4	No. 5	RMS
Experimental (m/s ²)	164.2	41.34	98.2	77.8	81.2	-
Analytical (m/s ²)	180.9	44.99	88.56	64.1	94.62	0.158

Empirical (m/s ²)	167.2	41.2	91.8	79.4	78.5	0.075
----------------------------------	-------	------	------	------	------	-------

3.6.2. Stress Analysis

PD of the material is modeled using analytical and numerical models in the previous sections. Besides PD, the stress level of the material is also very important for long term mechatronics applications. Therefore; the stress on the materials should also be studied. To analyze the stresses on the materials, two methods can be utilized. These methods are; a differential equation and FEM. The differential equation converts PD to the stress assuming a uniform stress distribution on the specimen. In other words, it neglects the shear stress at the corners. To solve this problem, numerical software, i.e. ANSYS 14.5, is utilized in this work.

3.6.2.1. Differential Equation

In this section, the differential equation of dynamic deceleration is derived to convert deceleration to the stress. Modeling of the viscoelastic elastomer as a spring and a damper is difficult due to its nonlinearities. Further, its mechanical properties change with the specimen size. Therefore, instead of dynamically analyzing the material, we used a methodology to convert the measured acceleration to the stress. In general, impact force of a viscoelastic material could be modeled as;

$$F = c\dot{x} + kx \quad (26)$$

where, k and c represent the stiffness and damping coefficient respectively. According to [34], the force on the material can be calculated as;

$$F = m\ddot{x} + mg \quad (27)$$

where m is the mass of the impact rig, g is the acceleration of the gravity and \ddot{x} is the deceleration measured by the accelerometer. If the equation is divided into the area of the specimen, the stress equation can be derived as;

$$\sigma = \frac{\sigma_0}{g} \ddot{x} + \sigma_0 \quad (28)$$

where, $\sigma_0 = \frac{mg}{A}$ is the static stress. The initial conditions of the equation of motion are:

$$x(0) = 0, \dot{x}(0) = \sqrt{2gH}, \ddot{x}(0) = g \quad (29)$$

where, H is the drop height. In addition, if the stresses are known, it can also be converted into the acceleration as well using the equation below;

$$\ddot{x} = \frac{g}{\sigma_0} (\sigma - \sigma_0) \quad (30)$$

3.6.2.2. Finite Element Method

In this section, the process of FEM using ANSYS is described in detail. The same element type is used to mesh all asymmetric 3-D specimens. The element type is selected as solid 20node186 for meshing the specimen and the impact rig; the element has a quadratic displacement behavior and characterized by 20nodes having three degrees of freedom on each node: translations in the nodal x , y , z directions. Moreover, because of the large deformation capabilities of the elements, it can be used for meshing hyperelastic and viscoelastic materials. For the sake of simplicity, other element type of 8node183 is used for symmetric specimens. The element has a quadratic displacement behavior and is defined by 8 nodes having two degrees of freedom at each node: translation in x and y directions. This element is suitable for

axisymmetric models. Further, it has a capability of simulating the nearly incompressible or fully incompressible hyperelastic materials.

In order to neglect the contact stiffness, Lagrange multiplier method was used to model the contact. After modeling and meshing, the contact elements could be selected automatically in ANSYS 14.5 by selecting the target line/surface and the contact line/surface. It should be notice that the impact rig is the moving object and must be selected as the contact surface and the specimen is fixed to the ground. The upper line/surface of the specimen must be selected as the target. CONTA174 and TARGE170 elements are selected for 3-D models and CONNTA 172 and TARGE169 elements are selected for 2-D models.

To analyze the dynamic behavior of the elastomer, ANSYS requires the definition of a hyperelastic material model. For this purpose, one of the nonlinear hyperelastic material models should be selected. In this work, Ogden material model is selected due to its nonlinear SED function. Constants of the material model are found by using hyperelastic curve fitting tool utilizing data-set of the multiple test set-ups (uniaxial tension, shear and biaxial tests) [21]. Details of preparation of each test data is described in the next section. Further, a nonlinear viscoelastic material model, William-Landel-Ferry (WLF) is selected as a shift function option. The WLF option should be used for polymeric materials. Finally, the Young's modulus of 210 (Gpa) and Poisson's ratio of 0.33 are defined as linear isotropic material model of the steel impact rig.

After modeling the polyurethane elastomer, all the parameters are inputted to ANYS. Figure 3.22 is the FE analysis result of a specimen with an area of 28.26 cm², thickness of 10 mm, drop weight of 2.663 kg and drop height of 50 cm. The model is analyzed in 2-D and then exhibited the ¾ expansion of axisymmetric model. As seen in Figure 3.22, the maximum stress occurs at the corners of the specimen because of the shear stress; however, the rest of the specimen exhibits almost a uniform stress. The Von-misses stress of the middle part of the specimen during an impact versus time is shown in Figure 3.23.

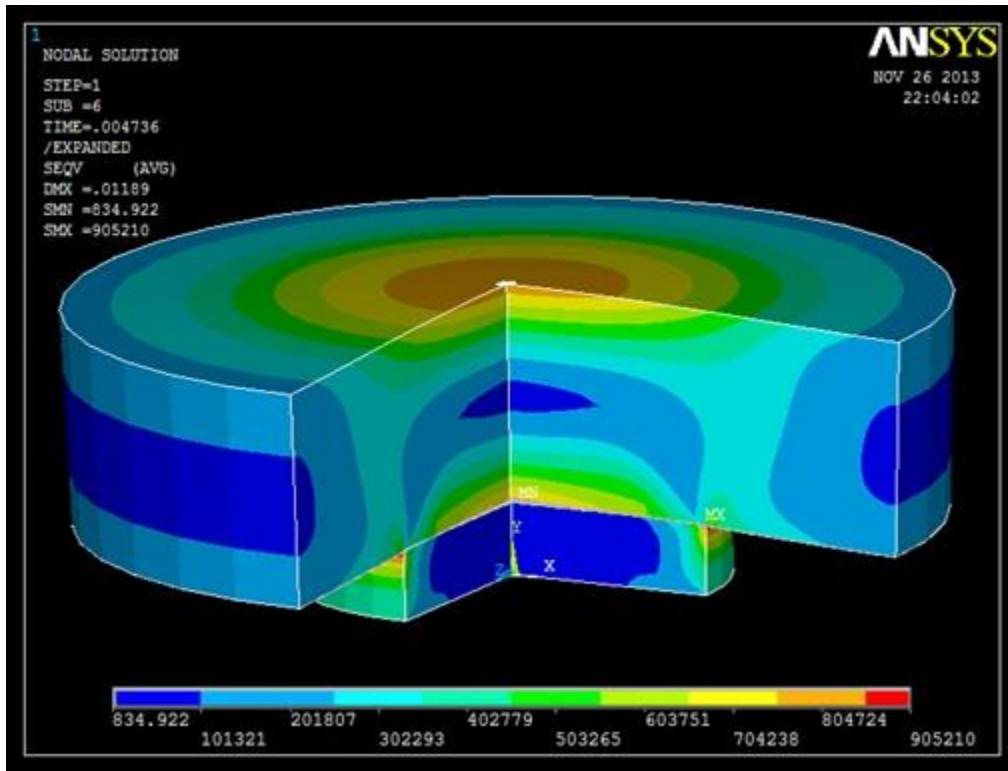


Figure 2421. 3-D analyzing the drop test in ANSYS

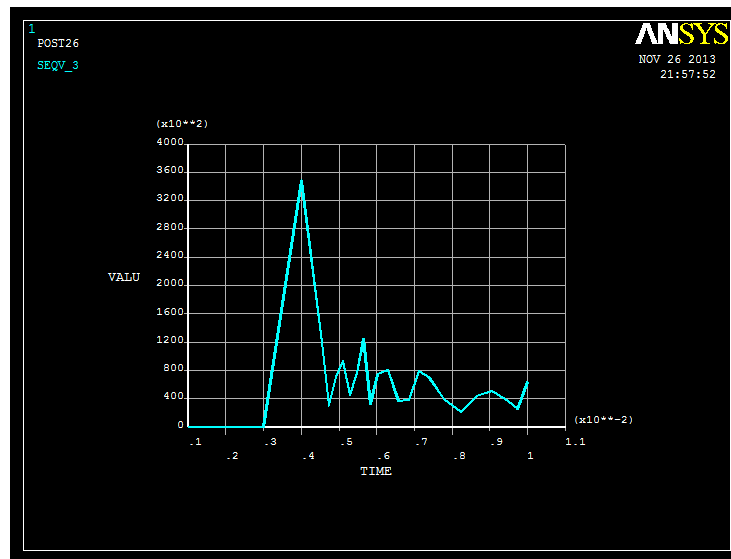


Figure 3.22. Von-mises stresses over time during an impact

3.6.2.3. Comparison of FEM and Differential Equation

The stress of the specimen in the middle calculated by FEM is compared with the differential equation results. Specimens listed in table 3.6 are used for this purpose. Figure 3.24 shows the comparison of FEM analysis and differential equation using data of experimental, analytical and empirical models.

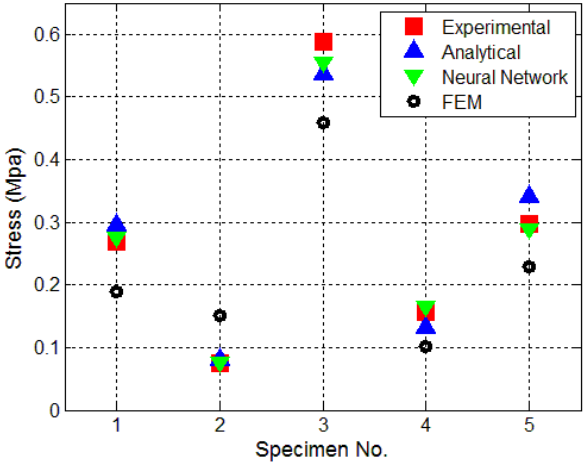


Figure 25. A plot of comparison of calculated stresses.

The correlation of mass is also shown to be a parameter which needs to be optimized depending on the application. For example; increasing the drop mass from 1.866 kg to 4.396 kg decreases the PD about 27%, however; increases the stress up to 43% as seen in Figure 3.18 and Figure 3.25 respectively.

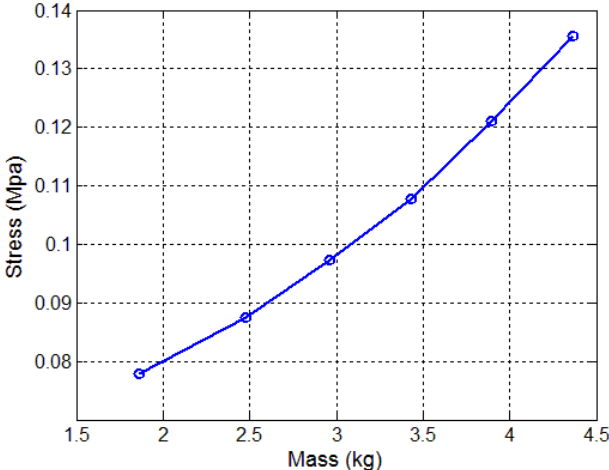


Figure 3.24. A plot of stress vs. mass

4. CONCLUSIONS

4.1. Improving SDM

Parameters which could affect mechanical properties (the maximum elongation and stress tolerance) such as mixing time and annealing are presented. Also mechanical properties change during days is presented. Further, it is found that bonding feature could be improved up to 20% by increasing cross sectional area of layers especially in a conic shape.

4.2. Analyzing a Hyperelastic Material using FEM

In this work, an estimation methodology is used to predict the data-set of pure shear and biaxial tension tests which are not practically performed as an experiment. For this purpose, the VL function is used to change the experimental stress-strain data-sets of uniaxial tension and uniaxial compression to the other test formats. Numerical analysis of the specimen under uniaxial tension and pure shear is evaluated by using four material models. Each material model behavior under different combination of inputted data-sets is compared with the related test experimental or estimated data-set. Finally, the uniaxial tension + biaxial and biaxial + pure shear data-sets combinations are observed to have the best convergence with the data-set of experimental uniaxial tension and estimated pure shear test respectively. It should be notice that:

- Three data-sets are used to create an ANSYS model. These models are; uniaxial tension experimental results and two estimated data-sets of shear and biaxial tests.
- Gent is proven to be the best material model for uniaxial tension test.
- Uniaxial tension + shear data-sets combination is proven to be the best combination for numerical analysis of a specimen under uniaxial tension test.
- Neo-Hookean is proven to be the best material model for pure shear test.
- Shear + biaxial data-sets combination is proven to be the best combination for numerical analysis of a specimen under pure shear test.

Finally, higher order Ogden model shows better results than Ogden 1rd as seen in Mooney-Rivlin in Figure 3.13.

4.3. Impact Analyzes of Viscoelastic Material

In this work, PD is measured utilizing an experimental drop test which is manufactured specifically for this task. Using the results of the drop tests, analytical and empirical PD models are developed. Then, new specimens, having different specimen size, are manufactured to compare the accuracy of models. It is seen that the NN method has better prediction than analytical model. It is shown that, these models enable us to predict the PD of a hypothetical specimen under hypothetical testing conditions without any further experimentation. Furthermore, stresses on the materials during impacts are calculated using derived differential equation. The equation uses the obtained PD data of experimental drop test, analytical and empirical models and change to stress; the results are compared with FEM. Differential equation could find the normal stress on the material and neglects the shear stress on the corners of specimen. However, FEM analysis shows the full spectrum of stresses throughout the specimen.

4.4. Future Works

Using the subjects discussed in this thesis, a rugged robot could be designed and manufactured.

In numerical analyzes of impact of the viscoelastic material, the Ogden model was considered as the hyperelastic material model. However, there are other material models such as Mooney-Rivlin, Neo-Hookean, Gent and etc. Each material model has a special strain energy density function which could affect the results. These material models use multiple test results (uniaxial tension, shear and biaxial) with different combinations (Uniaxial tension + Shear, Uniaxial tension + Biaxial, Shear + Biaxial, Uniaxial tension + Shear + Biaxial) to find the constants of each material model. In the next studies, the effects of these parameters should be studied. The same work can also be replicated for the other polyurethane elastomers for different

ranges depending on the application. Finally, real rugged robots should be manufactured and tested under real harsh conditions.

REFERENCES

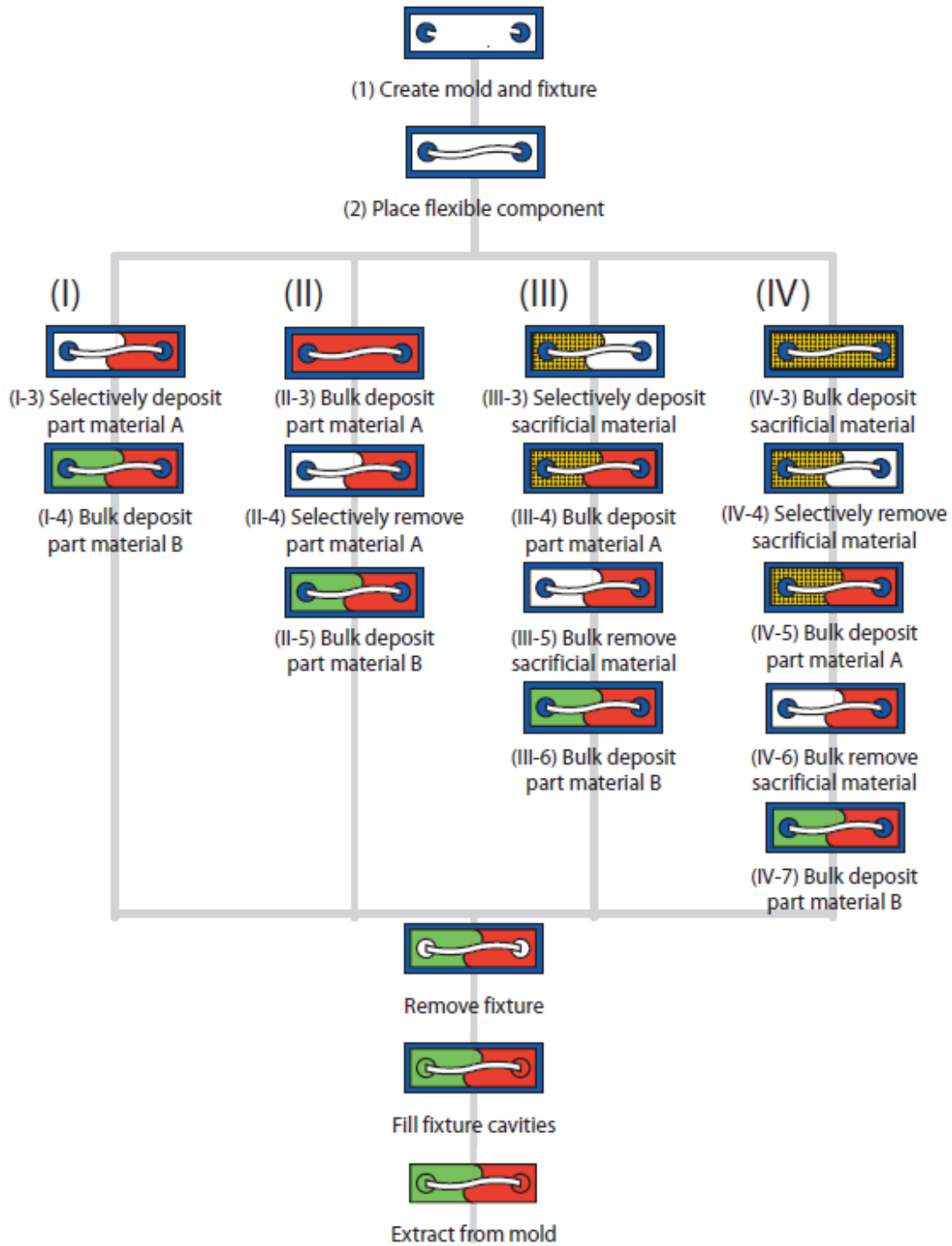
- [1] Boehme, B., Roellig, M., Wolter, K., Material Characterization of Organic Packaging Materials to Increase the Accuracy of FEM Based Stress Analysis, *Electronics System-Integration Technology Conference*, Greenwich, **2008**.
- [2] Chou, Ch., Hung, t., Yew, m., Yang, W., Hu, D., Tsai, m., Huang, ch., Chiang, K., Investigation of Stress-Bufler Enhanced Package Subjected to Board-level Drop Test, *Thermal, Mechanical and Multi-Physics Simulation and Experiments in Microelectronics and Micro-Systems*, Freiburg im Breisgau, **2008**.
- [3] Gung, L., Huang, H, W., Chiu, T.C., Lai, Y. S., Application of viscoelastic model for simulating process-induced war page of ball grid array packages, *Microsystems, Packaging, Assembly and Circuits Technology Conference*, Taipei, **2009**.
- [4] Alsakarneh, A., Moore, L., Barrett, J., Numerical Modelling and Optimization of an Electronic System Embedded in Multi-Layered Viscoelastic Materials under Shock Loads, *International Conference on thermal, mechanical and multiphysics simulation and experiments in microelectronics and microsystems*, EuroSimE. **2011**.
- [5] Sung, D. K., Modeling and Analysis of a Nonlinear Elastomer Impact Model with Damping Mechanism, *Korea advanced institute of science and technology*, Taejon, korea. **1991**.
- [6] Sherwood,J, A., FROST, C, C., Constitutive Modeling and Simulation of Energy Absorbing Polyurethane Foam under Impact Loading, *polymer engineering and science*, **1992**.
- [7] Thornhill, R, J., Smith, C, C., Impact Force Prediction Using Measured Frequency Response Functions, *Journal of dynamic systems, measurement, and control*, 105, **1983**.
- [8] Bergstrom, J, G., Boyce, M, C., Constitutive Modeling of Large Strain Time-Dependent Behavior of Elastomers, *Journal of the Mechanics and Physics Solid*, 46, 931-954, **1998**.
- [9] Gent, A. N., *Engineering with Rubber*, Oxford University Press, New York, **1992**.
- [10] Lee, S. J., Active, *Polymer Based Composite material Implementing Simple Shear*, PHD thesis, Texas A & M University, **2007**.

- [11] Ogden, R. W., Large Deformation Isotropic Elasticity - On the Correlation of Theory and Experiment for Incompressible Rubberlike Solids, *Proceedings of the Royal Society of London Series A, Mathematical and Physical Sciences*, 326,565-584, **1972**.
- [12] Park, B., Prinz, F, B., *Microscopic assemblies with SDM processing*, Department of Mechanical Engineering, Stanford University, USA.
- [13] Alsakraneh, A., Evaluation of the Use of a Rubber Buffer Layer to Protect Embedded SIP Devices from High Mechanical Forces, *IEEE*, 1883-1888, **2011**.
- [14] Li, J., Chen, X., Gao, D., Wang, Z., Establishment of Buffer Dynamic Model for Polyurethane Foam Cushion, *IEEE*, **2011**.
- [15] Kim, B., Lee, S, B.,LEE, J., Cho, S., Park, H., Yeom, S., Park, S, H.,A Comparison among Neo-Hookean Model, Mooney-Rivlin Model, and Ogden Model for Chloroprene Rubber, *International Journal of Precision Engineering and Manufacturing*, 13, 759-764, **2012**.
- [16] Jang,W, J., Lee,J., Woo, C, S., Kim, B, K., Lee, S B., An Experimental Study and Finite Element Analysis of Weatherstrip, *International Journal of Precision Engineering and Manufacturing*, 12, 97-104, **2011**.
- [17] Glucklich, J., Landel, R, F., Strain Energy Density Function of Styrene Butadiene Rubber and the Effect of Temperature, *Journal of Polymer Science*, 15, 2185-2199, **1977**.
- [18] Mckenna, G, B., Flynn, K, M., Chen, Y., Experiments on the Elasticity of Dry and Swollen Networks: Implications for the Frankel-Flory-Rehner Hypothesis, *American Chemical Society*, Vol. 22, No. 12, pp. 4507-4512, **1989**.
- [19] Kearsley, E, A.,Zapas, L, J., Some Methods of Measurement of an Elastic Strain-energy Function of The Valanis-Landel Type, *Journal of Rheology*, 24, 483-500, **1980**.
- [20] Bradley, G, L., Chang,P, C., Mckenna, G, B., Rubber Modeling Using Uniaxial Test Data, *Journal of Applied Polymer Science*, 81, 837-848, **2001**.
- [21] *Hyperelastic Material Curve Fitting*,. ANSYS Structural Analysis Guide for Release.
- [22] Mooney, M.,A Theory of Large Elastic Deformation, *Journal of Applied Physics*, pp. 582-592, **1940**.
- [23] *Nonlinear Finite Element Analysis of Elastomers*. MSC Software Co, Santa Ana.
- [24] Gent, A. N., A New Constitutive Relation for Rubber, *Rubber Chemistry Tech*, 59-61. **1996**.
- [25] Mullins, L., Effect of Stretching on the Properties of Rubber, *Rubber Chemistry and Technology*, 21, 281-300, **1948**.

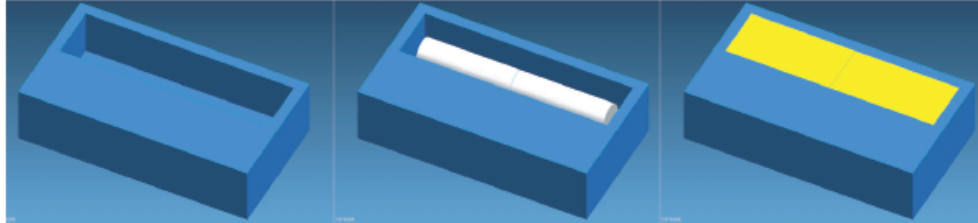
- [26] Manuel, J., Garcia, R., Oscar, E., Ruiz, R., Lopez, C., *Technical Report Hyperelastic Material Modeling*, **2005**.
- [27] Zoller, P., Instrumentation for Impact Testing of Plastics, *Polymer testing*, 197-208, **1983**.
- [28] Nairn, J. A., Measurement of Polymer Viscoelastic Response During an Impact Experiment, *Polymer engineering and science*, 29, **1989**.
- [29] Manufacture of a Double-Jointed, Compliant SDM Leg, http://www-cdr.stanford.edu/biomimetics/documents/double_joint/double_joint.html
- [30] Cooper, A. G., Kang, S., Kietzman, J. W., Prinz, F. B., Lombardi, J. L., Weiss, L. E., Automated Fabrication of Complex Molded Parts Using Mold Shape Deposition Manufacturing, *Materials and Design*, 20, 83-89, **1999**.
- [31] Solovitz, S. A., Eaton, J. K., Aeroelastic Control Using Redundant Microactuators, *Proceedings of the 3rd ASME/JSME Joint Fluids Engineering Conference*, San Francisco, California, **1999**.
- [32] Toyserkani, H., *Fundamentals of material science*, Publications of Isfahan University of technology, Isfahan, **2006**.
- [33] Hegan, M., *Neural Network Design*, **1996**.
- [34] Chen. X, Li .J, Gao. D, Wang. Zh., Establishment of Buffer Dynamic Model for Polyethylene Foam Cushion, *mechanic automation and control engineering*, **2011**.
- [35] Hatanaka, M., *Design and Fabrication of Multimaterial Flexible Mechanisms with Embedded Components*, PHD thesis, Stanford university, **2005**.

APPENDIX

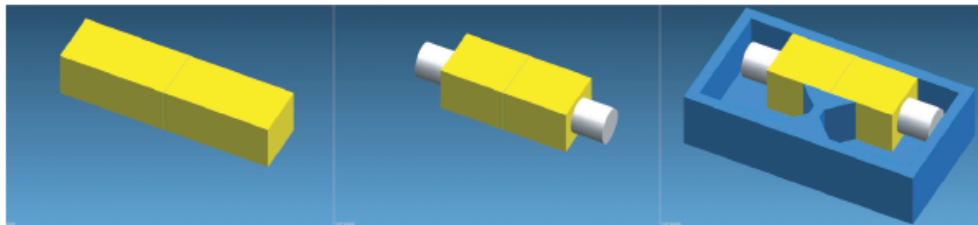
Appendix 1: four main manufacturing processes of SDM method [35]



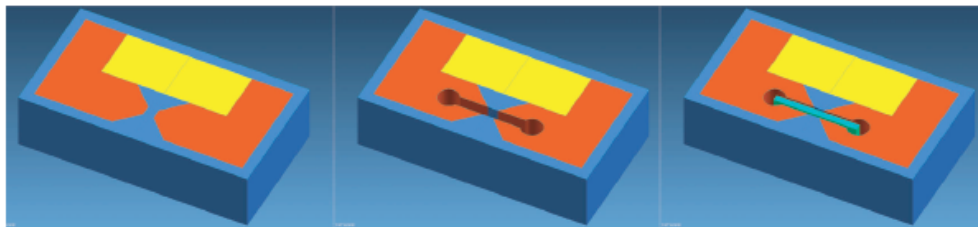
Appendix 2: The manufacturing process of a spring-loaded hinge [35]



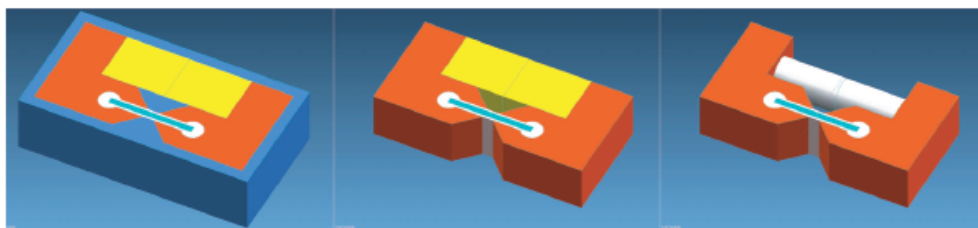
Machine mold in support material and place coil spring inside . Then bulk-deposit wax to protect the spring from being embedded in plastic.



Release the wax-encased spring from the mold and selectively remove wax from its ends to expose sections to be embedded in plastic. Replace in new mold.

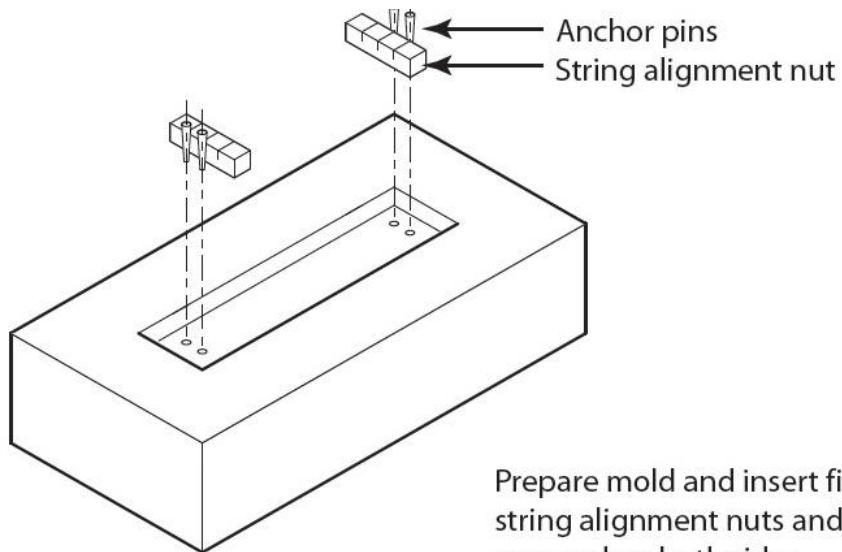


Bulk-deposit part material A in mold cavity and machine mold cavity for the flexure in the part material and mold. Insert reinforcement fabric in slot.

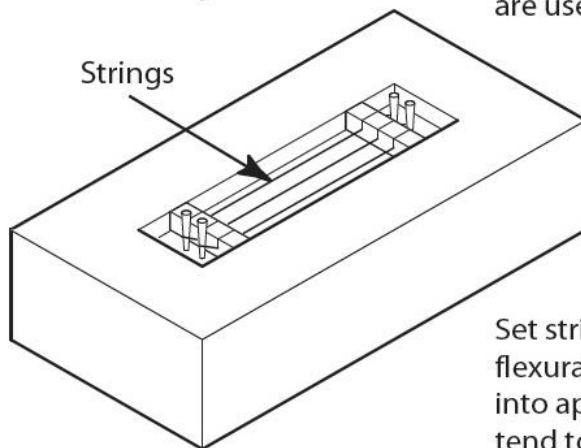


Bulk-deposit soft material B to encapsulate fabric. Extract part from mold and bulk-remove protective wax from coil spring by melting.

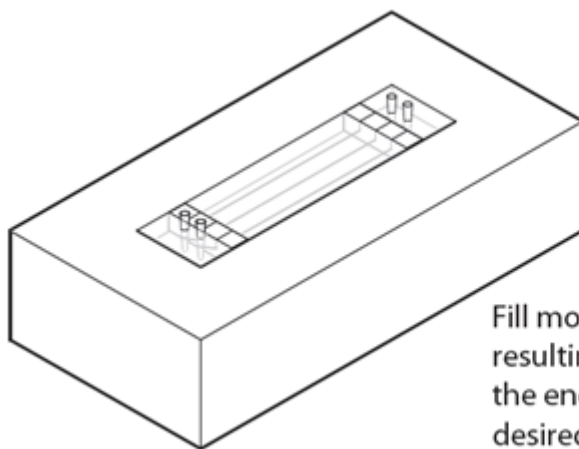
Appendix 3: Pre-encapsulation [35]



Prepare mold and insert fixtures. Here, string alignment nuts and anchor pins are used on both sides.

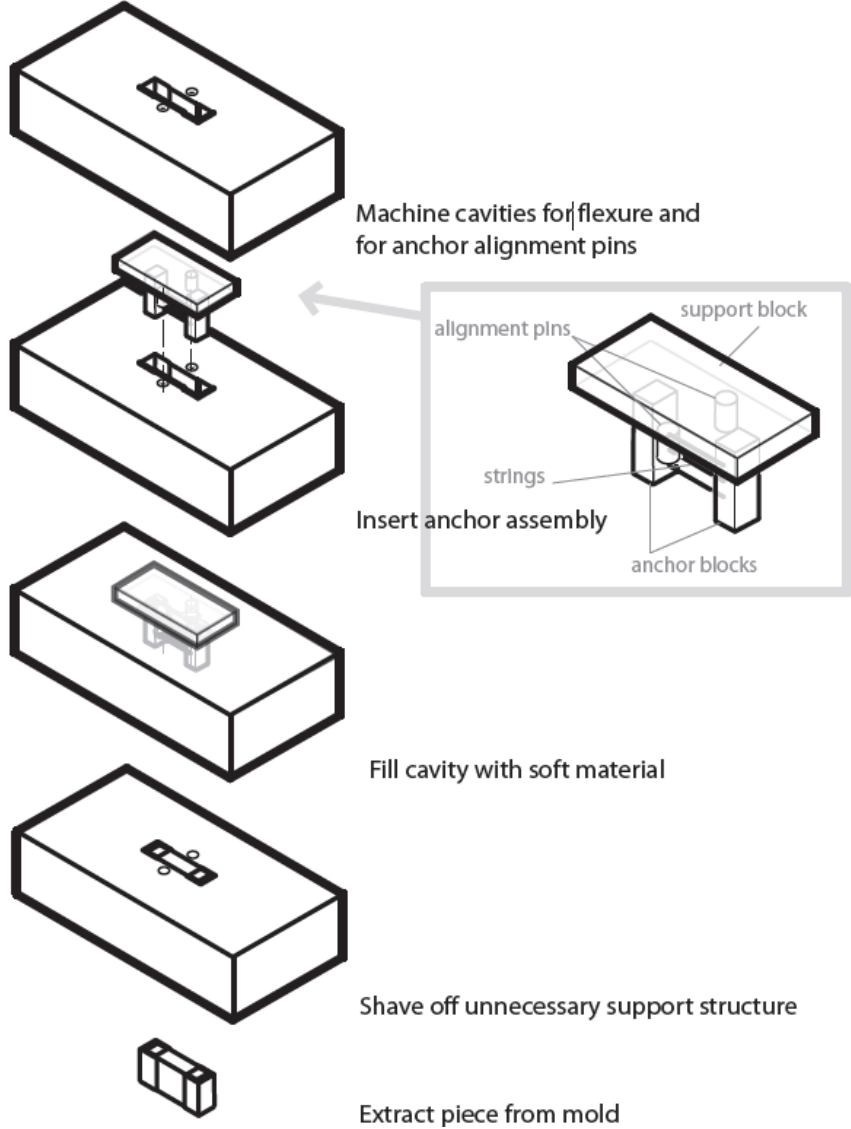


Set string in tension. Typically, longer flexural elements are made and cut into appropriate sizes. However, strings tend to float in the uncured polymer and be misplaced when they are too long.



Fill mold with polymer. Extract the resulting product from mold. Remove the end fixtures. Cut the product into desired lengths and use in other products.

Appendix 4: Suspending fixture method [35]



CURRICULUM VITAE

Credentials

Name, Surname : Behrang , Shamsadinlo
Place of Birth : Naghadeh
Marital Status : Single
E-mail : shamsadinlo@gmail.com
Address : Demetgül mihallesi, st.422, 6/48, Yenimühalle, Ankara

Education

High school : Kharazmi and Shariati highschoools
BSc. : Islamic Azad University of Tabriz (IAUT)

Foreign Languages

Turkish, English, Farsi, Arabic

Work Experience

Work experience in Bazsazi Locomotive Karaj

Areas of Experience

Finite Element Analysis, Design and Analysis of Pressure Equipment, Rapid Prototyping, Numerical and Analytical Analysis, Nonlinear Control

Publications

- Ali Shamsaddinlou, Akbar Tohidi, **Behrang Shamsadinlo**, “**Performance Increasing of Multiple Model Based Control**”, IEEE Multi-Conference on Systems and Control, India, August 28-30, 2013. (Accepted and to be Published).
- **Behrang shamsadinlo**, Mohammad Shakouri ghazani, “**Analyzing U-bolts Effects on Fatigue Failure of the Center Hole of a Leaf Spring**”, Hamayesh Farzan, Islamic Azad University of Tabriz, January 22-25, 2009 (Accepted and published in Persian)
- **Behrang Shamsadinlo**, Özgür Ünver, “**Analytical and Empirical Modeling of Peak Deceleration and Stress Analysis of Polyurethane Elastomer under Impact Loading Test**”, International journal of Precision engineering and manufacturing. (Submitted).